
PHYSICS-INSPIRED GENERATIVE MODELS IN MEDICAL IMAGING: A REVIEW

Dennis Hein^{*1,2}, Afshin Bozorgpour^{*3}, Dorit Merhof^{†3,4}, and Ge Wang^{†5}

¹Department of Physics, KTH Royal Institute of Technology, Stockholm, Sweden

²MedTechLabs, Karolinska University Hospital, Stockholm, Sweden

³Faculty of Informatics and Data Science, University of Regensburg, Regensburg, Germany

⁴Fraunhofer Institute for Digital Medicine MEVIS, Bremen, Germany

⁵Department of Biomedical Engineering, School of Engineering, Biomedical Imaging Center, Center for Biotechnology and Interdisciplinary Studies, Rensselaer Polytechnic Institute, Troy, NY, USA

ABSTRACT

Physics-inspired Generative Models (GMs), in particular Diffusion Models (DMs) and Poisson Flow Models (PFMs), enhance Bayesian methods and promise great utility in medical imaging. This review examines the transformative role of such generative methods. First, a variety of physics-inspired GMs, including Denoising Diffusion Probabilistic Models (DDPMs), Score-based Diffusion Models (SDMs), and Poisson Flow Generative Models (PFGMs and PFGM++), are revisited, with an emphasis on their accuracy, robustness as well as acceleration. Then, major applications of physics-inspired GMs in medical imaging are presented, comprising image reconstruction, image generation, and image analysis. Finally, future research directions are brainstormed, including unification of physics-inspired GMs, integration with Vision-Language Models (VLMs), and potential novel applications of GMs. Since the development of generative methods has been rapid, this review will hopefully give peers and learners a timely snapshot of this new family of physics-driven generative models and help capitalize their enormous potential for medical imaging.

Keywords Physics-inspired generative models, Bayesian Theorem, Diffusion Model, Poisson Flow Generative Model, PFGM++, Consistency Model, Medical Imaging, Image Reconstruction, Image Analysis, Image/Data Synthesis

1 INTRODUCTION

The Bayesian theorem, which is fundamental to many fields, is expressed as $P(A|B) = P(B|A)P(A)/P(B)$, where $P(A|B)$ is the posterior probability that event A will occur given that B is true, and $P(B|A)$ is the likelihood defined as the probability that event B will occur given that A is true. Many medical imaging problems are actually special cases of Bayesian inference. The Bayesian formula embodies the essence of rational decision-making under uncertainty, provides a rigorous framework to update our belief based on new evidence, and has led to numerous successes in major applications and even in philosophical arguments about the nature of knowledge and learning. By its quantifiable, coherent and powerful nature, the Bayesian approach elegantly serves as a cornerstone of modern science and technology.

In tomographic image reconstruction, A is an image to be reconstructed from tomographic data B . For many years, maximum a posteriori (MAP) image reconstruction has been the holy grail to reconstruct an optimal image that is most probable given the observed data and prior knowledge about the underlying images. By maximizing the posterior probability, MAP reconstruction balances the fidelity to the observed data with regularization imposed by the prior. However, it is well known that the main challenge in achieving the MAP reconstruction (and many other tasks) is often the lack of a good model for the distribution of A . Assuming $P(A)$ to be constant, the maximum likelihood estimation was widely used as a surrogate of the MAP estimation. To approximate $P(A)$, roughness penalty, sparsity constraint,

*Equal contributions

†Corresponding authors

and low-rank prior were subsequently introduced, but these classic regulators are quite simplistic, commonly expressed mathematically in no more than one line. Indeed, an image content A in the real world can have rather sophisticated and diverse features, being typically on a low-dimensional manifold. Until approximately one decade ago, modelling a highly complex data distribution has been an intractable task.

Currently, the landscape of artificial intelligence (AI) and machine learning, especially deep learning, is rapidly evolving, with generative AI at the forefront of innovation. Contemporary generative AI methods have revolutionized the field of AI and machine learning by enabling the creation of new, synthetic instances of data that are practically indistinguishable from real ones. These techniques have widespread applications, with Sora and GPT-4o as two amazing examples.

In retrospect, Variational Autoencoders (VAEs) and Generative Adversarial Networks (GANs) were among the first to pave the way. VAEs work by encoding input data into a lower-dimensional space and then synthesize samples in the original space, obeying the distribution of the original data. GANs, on the other hand, consist of two competing networks: a generator that creates data and a discriminator that separates generated and real data. The two networks interact to define the adversarial process that improves the quality of the generated data so that they are indistinguishable from the original data. More recently, physics-inspired Generative Models (GMs) have become the state of the art, with the Diffusion Models (DMs) and Poisson Flow Generative Models (PGFMs) being the most popular ones. They construct an image or sample by starting from a random distribution and refining it towards the distribution of the target data through a sampling process in a number of steps (from thousands in the original setting to one in the consistency model). These physics-inspired GMs can generate realistic, diverse, and complex data in a principled yet universal way, already demonstrating a huge potential for medical imaging. Notably, as we will see in this review, VAEs are making a silent comeback as a key construct playing a pivotal role in the state-of-the-art generative methods.

Given the importance and momentum of generative AI research, there are a good number of review papers already under this theme. We used the Scopus rule in the Article Title field “Survey OR Review OR Overview” and obtained 113 documents. After examination, not all these reviews are relevant to generative AI or of the same quality. Furthermore, these reviews are not up-to-date, given the rapid evolution of the field. Also, we have an excellent GitHub repository “Awesome-Diffusion-Models”, <https://github.com/diff-usion/Awesome-Diffusion-Models>, which is a comprehensive collection of curated documents dedicated to the study and application of diffusion-type models, including introductory posts, papers, videos, lectures, tutorials, and Jupyter notebooks on various aspects of such models. Based on our ScopusTM search results and this repository, in the following we comment on the most recent and most comprehensive reviews that are closely related to medical imaging.

An overview of DMs was first posted in November 2022, revised in June 2023, and formally published in Aug 2023 in *Medical Image Analysis* [56]. It cited 192 key papers and provides an in-depth coverage of the theoretical foundations of DMs, their practical applications in medical imaging using the taxonomy built on nine sub-fields such as image translation, reconstruction, and anomaly detection, as well as the challenges and future directions. The survey categorized DMs based on their applications, imaging modality, organ of interest, and algorithms, offering a multi-perspective categorization and highlighting the importance of these models in generating synthetic medical images. Such realistically simulated samples can alleviate data scarcity and improve network training for superior performance.

Another interesting review published in August 2023 analyzed 80 papers on image generation using DMs [124]. The difficulties were examined in generating images with multiple objects, creating images of rare/novel objects and improving quality of generated images. The paper organized the discussion around these challenges and presented various methods to address them, such as leveraging layout information, refining attention maps, and employing retrieval-based methods. It also touched upon the importance of text encoders in improving image quality and explored the use of mixtures of experts and reinforcement learning to enhance outcomes.

Another survey over 160 papers was posted in 2022 and published in *IEEE Transactions on Pattern Analysis and Machine Intelligence (TPAMI)* in September 2023 [28]. It covered DMs in the field of computer vision and addressed the three schemes: Denoising Diffusion Probabilistic Models (DDPMs), Noise Conditioned Score Networks (NCSNs), and Score-based Diffusion Models (SDMs) via stochastic differential equations (SDEs). The paper also discussed the relationship between DMs and other GMs, presenting a categorization of DMs applied in computer vision and identifying research directions, particularly the need to improve sampling/inference efficiency without compromising the quality of generated samples. In yet another comprehensive review of 258 papers on DMs in various domains, the core aspects were presented of the formulation, algorithms, and applications [13]. Through gradual refinement of the review from September 2022 (version 1) to December 2023 (version 10), this review highlighted methods for generating high-fidelity samples across different modalities and discussed strategies for sampling acceleration, diffusion process design, and likelihood optimization. The article was concluded with discussions on the current limitations and future advancements.

While each review had different methodological emphases and covered various spectra of applications, they have collectively underscored the significance of DMs across different fields, with the common core challenge to optimize the image quality and sampling efficiency individually or simultaneously.

While the above reviews/surveys are excellent and complementary, the rationale for us to write this new review is still compelling. Recently, especially over the past year, the emergence of PFGMs [113, 114] represents a significant leap forward in the field of generative AI, modeling complex data distributions and producing high-fidelity samples with the state-of-the-art performance. Like DMs, Poisson flow or other physics-/mathematics-inspired GMs can be cast in the score-matching format. Unlike DMs, which draw their inspiration from non-equilibrium thermodynamics, PFGM are grounded in the principle of electrostatics, bringing new theoretical insights and empowering technical capabilities. This foundational shift offers a distinct advantage in terms of precision and efficiency. Poisson equations allow for a more direct manipulation of the data distribution, enabling a better controlled and potentially faster convergence to the target distribution. At the same time, impressive new results have been reported on the classic DMs such as consistency models. Therefore, the benefits to thoroughly summarize and analyze these advancements through a new review article are clear; mainly, to clarify the new thinking and mechanisms, capitalize the theoretical and technical potentials, and facilitate real-world applications of contemporary generative AI.

In preparing this review, we made our best effort in the literature search using various platforms and databases. In addition to Scopus and the GitHub repository we have mentioned above, we have also used PubMed, Google Scholar, arXiv, as well as proceedings of relevant conferences such as ICLR and NeurIPS. To visualize this booming field, in Figure 1 (a)-(d) we show our ScopusTM search results with the rule in the field of Article Title, Abstract, and Key Words: “(Diffusion OR (Poisson AND flow)) AND (AI OR (Artificial AND Intelligence) OR (Deep AND Learning)) AND (Deep AND Network)”, which yielded 2,811 documents in total on June 28, 2024. Then, using the open-source software tool VOSviewerTM, we further analyze the bibliometric results in terms of co-occurrence of key words to produce Figure 1 (e).

The rest of this review is organized as follows. In the second section, physics-driven GMs are critically described from DMs to PFGM++, along with cutting-edge techniques for accelerated inference. In the third section, medical imaging applications of these GMs are concisely summarized, involving image reconstruction, image generation, and image analysis. In the last section, future directions are openly discussed, as related to unification of physics-inspired GMs, integration with VLMs, and potential novel applications of GMs.

2 PHYSICS-INSPIRED GENERATIVE MODELS

In this section, we give an overview of physics-inspired GMs, going from the earlier versions of DMs based on Markov chains all the way to the latest developments employing a combination of a score matching loss, distillation loss, and an adversarial loss to achieve state-of-the-art image quality and sampling efficiency. In doing so, we will place a particular emphasis on the generalized framework referred to as PFGM++ [114], as this takes a key step towards the unification of physics-inspired GMs.

2.1 DDPMs

DDPMs [83, 48] are a class of GMs that have gained significant attention for their ability to generate high-quality images without adversarial training. The core idea behind DDPMs is to model the generation process as an iterative denoising process over a sequence of time steps, starting from pure noise and progressively adding structure to reach a sample from the data distribution. More formally, for each training data point $\mathbf{x}_0 \sim p(\mathbf{x})$ a discrete Markov chain $\mathbf{x}_0, \mathbf{x}_1, \dots, \mathbf{x}_N$ is constructed with transition kernel $p(\mathbf{x}_i | \mathbf{x}_{i-1}) = \mathcal{N}(\mathbf{x}_i; \sqrt{\alpha_i} \mathbf{x}_i, (1 - \alpha_i) \mathbf{I})$ for $\alpha_i := \prod_{j=1}^i (1 - \beta_j)$. A sequence of positive noise scales $0 < \beta_1, \beta_2, \dots, \beta_N < 1$ will be chosen such that \mathbf{x}_N are approximately distributed as $\mathcal{N}(\mathbf{0}, \mathbf{I})$. The reverse variational Markov chain is parameterized as $p_\theta(\mathbf{x}_{i-1} | \mathbf{x}_i) = \mathcal{N}(\mathbf{x}_{i-1}; \frac{1}{\sqrt{1-\beta_i}}(\mathbf{x}_i + \beta_i s_\theta(\mathbf{x}_i, i)), \beta_i \mathbf{I})$ and is learned through the objective:

$$\theta^* = \arg \min_{\theta} \sum_{i=1}^N (1 - \alpha_i) \mathbb{E}_{p(\mathbf{x})} \mathbb{E}_{p_{\alpha_i}(\tilde{\mathbf{x}} | \mathbf{x})} [\|s_\theta(\tilde{\mathbf{x}}, i) - \nabla_{\tilde{\mathbf{x}}} \log p_{\alpha_i}(\tilde{\mathbf{x}} | \mathbf{x})\|_2^2], \quad (1)$$

where $p_{\alpha_i}(\tilde{\mathbf{x}}) := \int p(\mathbf{x}) p_{\alpha_i}(\tilde{\mathbf{x}} | \mathbf{x}) d\mathbf{x}$ denotes the perturbed data distribution. Once equipped with an estimation of the minimizer in Equation (1) a sample is generated by the reverse Markov chain

$$\mathbf{x}_{i-1} = \frac{1}{\sqrt{1-\beta_i}}(\mathbf{x}_i + \beta_i s_{\theta^*}(\mathbf{x}_i, i)) + \sqrt{\beta_i} \mathbf{z}_i, i = N, N-1, \dots, 1, \quad (2)$$

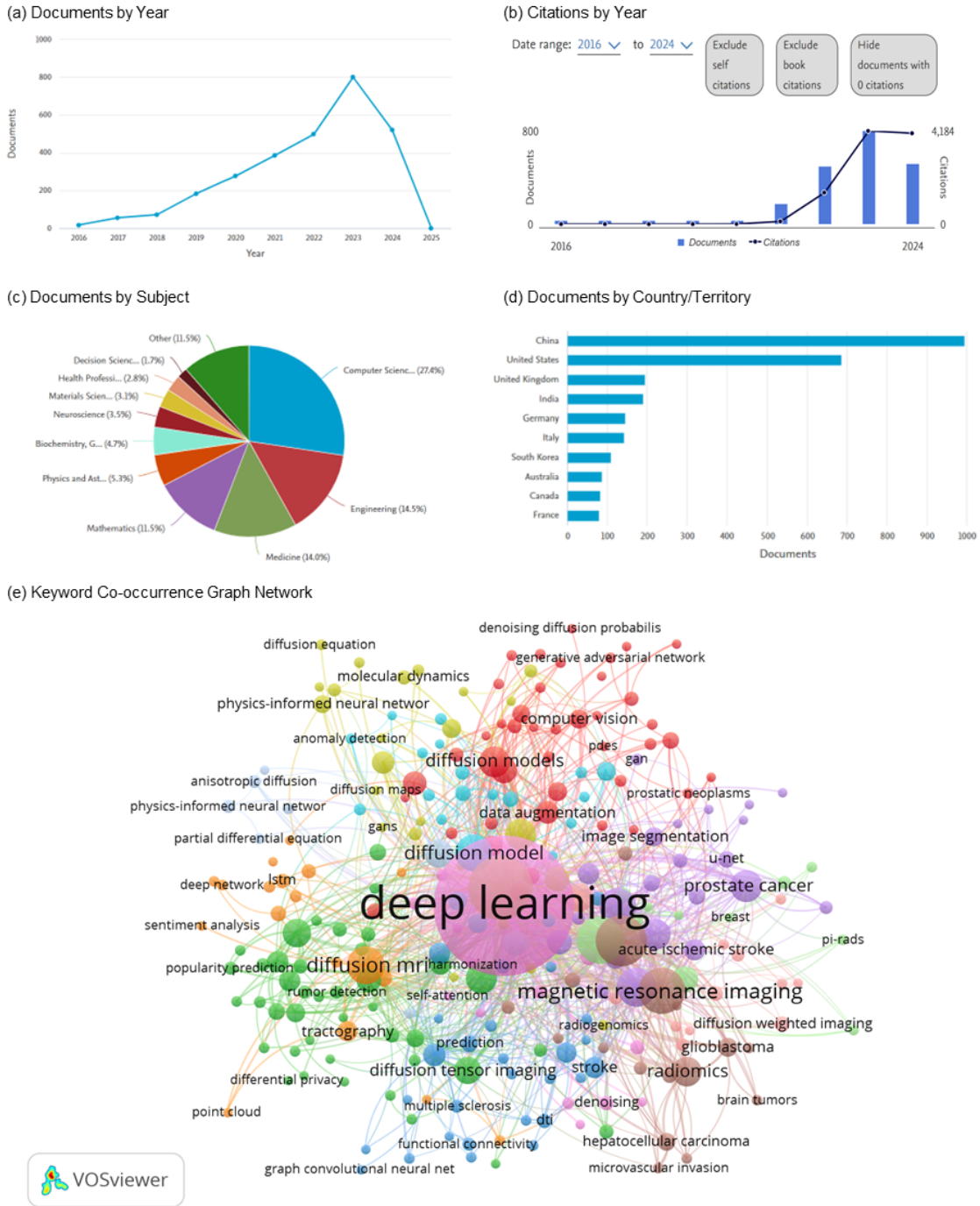


Figure 1: Scopus™ search results on diffusion-type generative AI models. (a) The number of diffusion-type generative AI papers; (b) the number of citations of these papers; (c) applications of diffusion-type generative AI models in various fields; (d) contributions from top countries and territories; and (e) a VOSviewer™ presentation in terms of authors' key-words co-occurrences. With a threshold of 5 co-occurrences, 258 key words were selected to form this graph network.

starting from $\mathbf{x}_N \sim \mathcal{N}(\mathbf{0}, \mathbf{I})$. The key to the success of DDPMs is that they transform the problem of generating samples from complex data distributions into a sequence of simpler denoising tasks, enabling high-quality image generation without adversarial training.

2.2 NCSNs

NCSNs [87] are a type of GM that leverage score-based generative modeling to produce high-quality synthetic samples. The fundamental concept of NCSNs involves learning the score of the data distribution conditioned on different noise scales, rather than directly learning the distribution itself. As for DDPM, let $p_\sigma(\mathbf{x}) := \int p(\mathbf{x})p_\sigma(\tilde{\mathbf{x}}|\mathbf{x})d\mathbf{x}$ denote the perturbed data distribution and $p_\sigma(\tilde{\mathbf{x}}|\mathbf{x}) := \mathcal{N}(\mathbf{x}, \sigma^2\mathbf{I})$ the perturbation kernel. We then choose a sequence of positive noise scales $\sigma_{\min} = \sigma_1, \sigma_2, \dots, \sigma_N = \sigma_{\max}$ such that $p_{\sigma_{\min}}(\mathbf{x}) \approx p(\mathbf{x})$ and $p_{\sigma_{\max}}(\mathbf{x}) \approx \mathcal{N}(\mathbf{x}; \mathbf{0}, \sigma_{\max}^2\mathbf{I})$. NCSNs then estimate a score network $s_\theta(\mathbf{x}, \sigma)$ via the denoising score matching (DSM) [100] objective

$$\theta^* = \arg \min_{\theta} \sum_{i=1}^N \sigma_i^2 \mathbb{E}_{p(\mathbf{x})} \mathbb{E}_{p_{\sigma_i}(\tilde{\mathbf{x}}|\mathbf{x})} [\|s_\theta(\tilde{\mathbf{x}}, \sigma_i) - \nabla_{\tilde{\mathbf{x}}} \log p_{\sigma_i}(\tilde{\mathbf{x}}|\mathbf{x})\|_2^2]. \quad (3)$$

Using the estimated score network, a sample is generated by the M -step Langevin MCMC sampler

$$\mathbf{x}_i^m = \mathbf{x}_i^{m-1} + \epsilon_i s_{\theta^*}(\mathbf{x}_i^{m-1}, \sigma_i) + \sqrt{2\epsilon_i} \mathbf{z}_i^m, m = 1, 2, \dots, M, \quad (4)$$

where $\epsilon_i > 0$ denotes the step size, starting from an initial sample $\mathbf{x}_N \sim \mathcal{N}(\mathbf{0}, \sigma_{\max}^2\mathbf{I})$.

2.3 SDMs

SDMs [89], also known as score-based GMs, provide a unified framework for score-based models [87] and DMs [83, 48] by formulating the diffusion process as a stochastic differential equation (SDE). Intuitively, this takes the idea of perturbing the data and learning to model complex data distributions via a sequence of simpler denoising task to the limit where the number of noise scales becomes infinite, leveraging advances in score modelling to obtain an effective sequential denoiser. This SDE takes can be written on the general form

$$d\mathbf{x} = \boldsymbol{\mu}(\mathbf{x}, t)dt + g(t)d\mathbf{w}, \quad (5)$$

where $\boldsymbol{\mu}(\cdot, t)$ and $g(\cdot)$ are the drift and diffusion coefficients, respectively, and \mathbf{w} is the standard Wiener process. One can choose the drift and diffusion coefficients, and T , such that \mathbf{x}_T is some unstructured, easy to sample, noise distribution. Amazingly, according to the Anderson's theorem [4], the forward diffusion process has a corresponding reverse-time diffusion process, also a SDE, on the form

$$d\mathbf{x} = [\boldsymbol{\mu}(\mathbf{x}, t) - g(t)^2 \nabla_{\mathbf{x}} \log p_t(\mathbf{x})]dt + g(t)d\bar{\mathbf{w}}, \quad (6)$$

where $\bar{\mathbf{w}}$ now is the standard Weiner process in reverse time. Crucially, the reverse-time SDE only depends on the data distribution via the gradient of the log-likelihood, known as the score function. An illustration of the forward and reverse processes is available in Figure 2 (a). Corresponding to the reverse-time SDE, there is an ODE called the probability flow (PF) ODE [89]:

$$d\mathbf{x} = \left[\boldsymbol{\mu}(\mathbf{x}, t) - \frac{1}{2}g(t)^2 \nabla_{\mathbf{x}} \log p_t(\mathbf{x}) \right] dt. \quad (7)$$

As with NSCNs, the score function estimated via a DSM objective. Notably, as stated above, this frameworks includes DDPM and NCSN as special cases as they can be regarded as discretizations of two particular SDEs.

The framework in Karras et al. [54], which further builds on [89], describes the sampling process as moving along the PF ODE

$$d\mathbf{x} = -\dot{\sigma}(t)\sigma(t)\nabla_{\mathbf{x}} \log p_{\sigma(t)}(\mathbf{x})dt, \quad (8)$$

where $\sigma(t)$ is a predefined, time-dependent, noise scale and $\nabla_{\mathbf{x}} \log p_{\sigma(t)}(\mathbf{x})$ is the time-dependent score function of the perturbed data distribution. This PF ODE corresponds to specific choices in the more general form presented in Equation (7). In particular, we can move from Equation (7) to Equation (8) by setting $\boldsymbol{\mu}(\cdot, t) = \mathbf{0}$, $\sigma(t) = t$, and $g(t) = \sqrt{2t}$. Moving the ODE forward and backward in time, respectively, nudges the sample away from and towards the data distribution. Let $p(\mathbf{y})$ denote the data distribution, $p(\sigma)$ the training distribution of noise scales, $\lambda(\sigma)$ a weighting function, and $p_\sigma(\mathbf{x}|\mathbf{y}) = \mathcal{N}(\mathbf{x}, \sigma^2\mathbf{I})$ a Gaussian perturbation kernel, which samples perturbed versions \mathbf{x} of ground truth data \mathbf{y} . Then, the time-dependent score function is learned via the DSM objective, or perturbation based, objective

$$\mathbb{E}_{\sigma \sim p(\sigma)} \mathbb{E}_{\mathbf{y} \sim p(\mathbf{y})} \mathbb{E}_{\mathbf{x} \sim p_\sigma(\mathbf{x}|\mathbf{y})} [\lambda(\sigma) \|f_\theta(\mathbf{x}, \sigma) - \nabla_{\mathbf{x}} \log p_\sigma(\mathbf{x}|\mathbf{y})\|_2^2]. \quad (9)$$

Once equipped with this estimate, we can generate an image by drawing an initial sample from the prior noise distribution and solving Equation (8) using some numeric ODE solver. SDMs offer a powerful and elegant framework for generative modeling, leveraging the mathematics of diffusion processes and score functions to transform noise into high fidelity samples.

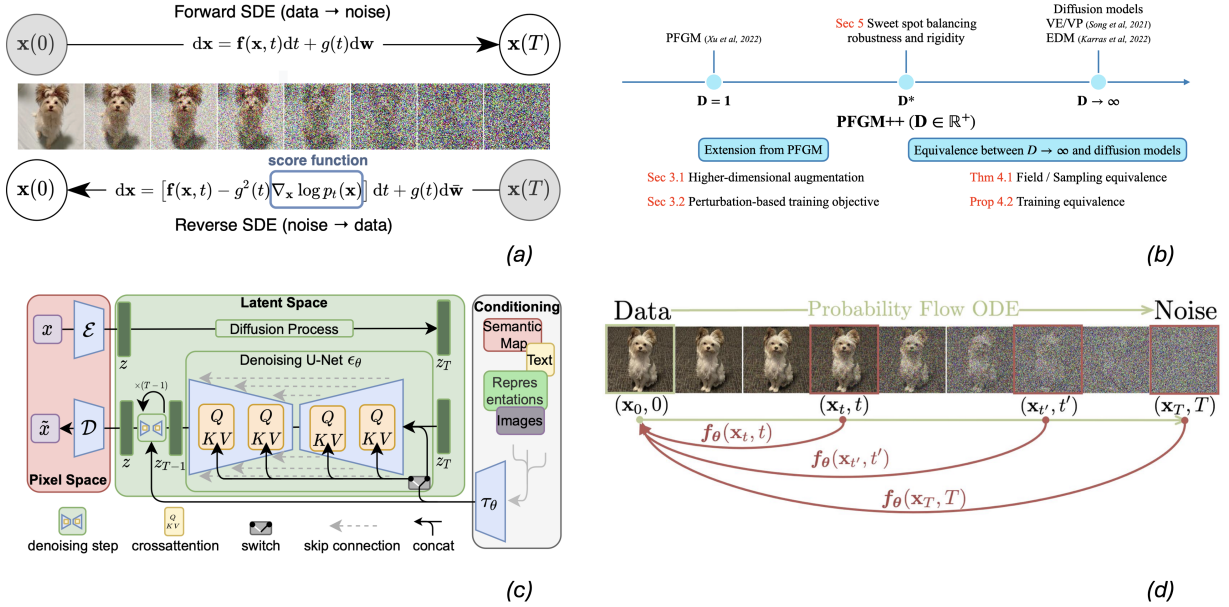


Figure 2: Physics-inspired deep GMs. (a) Schematic of forward and reverse SDE on SDMs [89]; (b) Overview of PFGM++ [114]; (c) Schematic overview of LDM [76]; (d) Schematic of mapping learned by consistency models [90]. Note that different notation may have been used in the text compared to this figure.

2.4 PFGMs

PFGMs [113] are a relatively new family of deep GMs inspired by electrostatics, instead of non-equilibrium thermodynamics as is the case for DMs. In particular, PFGMs treat the N -dimensional data $x \in \mathbb{R}^N$, as electric charges in a $N + 1$ -dimensional augmented space $\tilde{x} := (x, z) \in \mathbb{R}^{N+1}$. Following the law of motion defined by the electric field line emitted by the charges, the data distribution placed on the $z = 0$ hyperplane can be transformed into a distribution on the hemisphere with radius r . As $r \rightarrow \infty$ this distribution will become uniform [113]. Instead of estimating a time-dependent score function, as in SDMs, PFGMs learn an empirical Poisson field, derived from the Poisson equation in the augmented space,

$$\mathbf{E}(\tilde{x}) = \frac{1}{S_N(1)} \int \frac{\tilde{x} - \tilde{y}}{\|\tilde{x} - \tilde{y}\|^{N+1}} p(\mathbf{y}) d\mathbf{y}, \quad (10)$$

where $p(\mathbf{y})$ is the data distribution and $S_N(1)$ denotes the surface area of a unit N -sphere. We can move from the data distribution to the uniform distribution on the infinite hemisphere by running the ODE $d\tilde{x} = \mathbf{E}(\tilde{x})dt$ forward and back in time. In practice, PFGMs are trained using a large batch of size n to approximate the integral in Equation (10) to estimate a normalized empirical Poisson field $\hat{\mathbf{E}}(\tilde{x}) = c(\tilde{x}) \sum_{i=1}^n \frac{\tilde{x} - \tilde{y}_i}{\|\tilde{x} - \tilde{y}_i\|^{N+1}}$. The training objective is to minimize the ℓ_2 -loss between the network $f_\theta(\tilde{x})$ and $\mathbf{E}(\tilde{x})/\|\mathbf{E}(\tilde{x})\|$ over various, carefully selected to ensure coverage of sampling trajectories, positions of \tilde{x} . PFGMs represent a powerful approach to generative modeling, combining the stochastic modeling capabilities of Poisson processes with flow-based generative techniques.

2.5 PFGM++

PFGM++ [114] take an important step towards unification of physics-inspired GMs since it contains PFGMs [113] and, remarkably, SDMs [89, 54] as special cases. An overview is available in Figure 2 (b). PFGM++ in essence generalize PFGMs in terms of augmented space dimensionality. The N -dimensional data, $x \in \mathbb{R}^N$, are treated as positive electric charges in a $N + D$ -dimensional augmented space. Let $\tilde{x} := (x, z) \in \mathbb{R}^{N+D}$ and $\tilde{y} := (x, \mathbf{0}) \in \mathbb{R}^{N+D}$ denote the augmented perturbed and ground truth data, respectively. The electric field lines generated by these charges define a surjection via the ODE, $d\tilde{x} = \mathbf{E}(\tilde{x})dt$, between an uniform distribution on the infinite $N + D$ -dimensional hemisphere and the data placed on the $z = \mathbf{0}$ hyperplane. The objective of interest in PFGM++ is the high dimensional electric field

$$\mathbf{E}(\tilde{x}) = \frac{1}{S_{N+D-1}(1)} \int \frac{\tilde{x} - \tilde{y}}{\|\tilde{x} - \tilde{y}\|^{N+D}} p(\mathbf{y}) d\mathbf{y}, \quad (11)$$

where $S_{N+D-1}(1)$ is the surface area of the unit $(N + D - 1)$ -sphere, and $p(\mathbf{y})$ the ground truth data distribution. Xu et al. [114] note that the electric field is rotationally symmetric on the D -dimensional cylinder $\sum_{i=1}^D z_i^2 = r^2, \forall r > 0$ and it suffices to track the norm of the augmented variables $r(\tilde{\mathbf{x}}) := \|\mathbf{z}\|_2$. In particular, we can observe that

$$\frac{dr}{dt} = \sum_{i=1}^D \frac{z_i}{r} \frac{dz_i}{dt} = \frac{1}{S_{N+D-1}(1)} \int \frac{r}{\|\tilde{\mathbf{x}} - \tilde{\mathbf{y}}\|^{N+D}} p(\mathbf{y}) d\mathbf{y}, \quad (12)$$

where $dz_i = \mathbf{E}(\tilde{\mathbf{x}})_{z_i} dt$, and $\mathbf{E}(\tilde{\mathbf{x}})_{z_i}$ denotes the z_i component of $\mathbf{E}(\tilde{\mathbf{x}})$. For notational brevity, we can redefine $\tilde{\mathbf{y}} := (\mathbf{y}, 0) \in \mathbb{R}^{N+1}$ and $\tilde{\mathbf{x}} := (\mathbf{x}, r) \in \mathbb{R}^{N+1}$. The ODE of interest is then

$$d\mathbf{x} = \mathbf{E}(\tilde{\mathbf{x}})_{\mathbf{x}} \cdot E(\tilde{\mathbf{x}})_r^{-1} dr, \quad (13)$$

where $E(\tilde{\mathbf{x}})_r = \frac{1}{S_{N+D-1}(1)} \int \frac{r}{\|\tilde{\mathbf{x}} - \tilde{\mathbf{y}}\|^{N+D}} p(\mathbf{y}) d\mathbf{y}$, a scalar. Crucially, this symmetry reduction has converted the aforementioned surjection into a bijection between the ground truth data placed on the $r = 0$ ($\mathbf{z} = \mathbf{0}$) hyperplane and a distribution on the $r = r_{\max}$ hyper-cylinder [114]. For formal statement and proof see Theorem 3.1. in Xu et al. [114]. PFGM++ address several drawbacks of the training objective used in PFGMs by proposing a perturbation based objective, inspired by the DSM objective successfully used in SDMs [89, 54]. Let $p_r(\mathbf{x}|\mathbf{y})$ denote the perturbation kernel and $p(r)$ the training distribution over r . Then the objective can be formulated as

$$\mathbb{E}_{r \sim p(r)} \mathbb{E}_{p(\mathbf{y})} \mathbb{E}_{p_r(\mathbf{x}|\mathbf{y})} \left[\left\| f_{\theta}(\tilde{\mathbf{x}}) - \frac{\mathbf{x} - \mathbf{y}}{r/\sqrt{D}} \right\|_2^2 \right]. \quad (14)$$

For $p_r(\mathbf{x}|\mathbf{y}) \propto 1/(\|\mathbf{x} - \mathbf{y}\|_2^2 + r^2)^{\frac{N+D}{2}}$, it is possible to show that the minimizer of Equation (14) is $f_{\theta}^*(\tilde{\mathbf{x}}) = \sqrt{D} \mathbf{E}(\tilde{\mathbf{x}})_{\mathbf{x}} \cdot E(\tilde{\mathbf{x}})_r^{-1}$. Since the perturbation kernel is isotropic, one can sample from $p_r(\cdot|\mathbf{y})$ by splitting it into hyperspherical coordinates to $\mathcal{U}_{\psi}(\psi) p_r(R)$, where \mathcal{U}_{ψ} denotes the uniform distribution of the angle component and the distribution of $R = \|\mathbf{x} - \mathbf{y}\|$, the radius, is

$$p_r(R) \propto \frac{R^{N-1}}{(R^2 + r^2)^{\frac{N+D}{2}}}. \quad (15)$$

Once equipped with the minimizer of Equation (14), we can generate a sample from our target distribution by solving $d\mathbf{x}/dr = \mathbf{E}(\tilde{\mathbf{x}})_{\mathbf{x}}/E(\tilde{\mathbf{x}})_r = f_{\theta}^*(\tilde{\mathbf{x}})/\sqrt{D}$ with an initial sample from $p_{r_{\max}}$.

2.5.1 PFGM++ and SDMs in theory and in practice

PFGM++ admit PFGMs [113] ($D = 1$) and, remarkably, SDMs [89, 54] ($D \rightarrow \infty$) as special cases. In addition to being intimately connected in theory, PFGM++ and SDMs [89, 54] are also closely connected in practice. Xu et al. [114] demonstrate that one can re-purpose the training and sampling algorithms developed for DMs in [54] to PFGM++. This follows from the fact that $\sigma := \sigma(t) = t$ in [54], $\tilde{\mathbf{x}} := (\mathbf{x}, r)$, and the alignment formula $r = \sigma\sqrt{D}$, which allows for the change-of-variables $d\mathbf{x} = f_{\theta}^*(\tilde{\mathbf{x}})/\sqrt{D} dr = f_{\theta}^*(\tilde{\mathbf{x}}) dt$ since $dr = d\sigma\sqrt{D} = dt\sqrt{D}$.

2.5.2 Trade-off robustness for rigidity by varying D

In PFGM++, D is treated as a hyperparameter to be tuned. In particular, Xu et al. [114] demonstrate that by tuning $D \in (0, \infty)$ one can trade off robustness (insensitive to missteps) for rigidity (effective learning). In particular, as first shown for PFGM [113], PFGM++ are less susceptible to estimation errors than SDMs. Xu et al. [114] demonstrate the superior robustness of PFGM++ to three sources of errors: noise injection, large step-size, and post-training quantization. At training time, for large D and r , the marginal distribution $p_r(\mathbf{x})$ is supported on a sphere with radius $r\sqrt{N/D}$. If the sample trajectory deviates from this r -norm relation in the training data, the backward ODE can lead to unexpected results. Hence, setting D small, moving away from SDMs, increase robustness. However, a small D results in a heavy-tailed input distribution and a broad input range is challenging to handle for any finite capacity network. Thus, optimal performance occurs for some $D \in (0, \infty)$ that requires tuning for the problem at hand.

2.6 Latent DMs (LDMs)

LDMs [76] innovate by operating in a latent space—a compressed representation of the data—rather than directly in the data’s original space. This method significantly reduces computational costs while maintaining, or even enhancing, the quality of generated samples. In particular, [76] suggest a perceptual image compression via an autoencoder trained with a combination of perceptual and adversarial objectives. For a RGB image $\mathbf{x} \in \mathbb{R}^{H \times W \times 3}$ the encoder \mathcal{E}

encodes \mathbf{x} into the latent representation $\mathbf{z} = \mathcal{E}(\mathbf{x}) \in \mathbb{R}^{h \times w \times c}$. The decoder \mathcal{D} reverse this process, reconstructing the image from its latent representation $\tilde{\mathbf{x}} = \mathcal{D}(\mathcal{E}(\mathbf{x}))$. Rombach et al. [76] investigate a range of down-sampling factors $f = H/h = W/h$ and finds that $f = \{4, 8\}$ yields a good trade-off between computational complexity and image fidelity. In addition, Rombach et al. [76] introduce a very general conditioning mechanism to model conditional distributions $p(\mathbf{z}|\mathbf{y})$ by augmenting the DM backbone with a cross-attention mechanism [98], allowing the network to efficiently learn embeddings from varying modalities via domain specific encoders $\tau_{\theta}(\mathbf{y}) \in \mathbb{R}^{M \times d_{\tau}}$. A schematic overview of LDMs is available in Figure 2 (c).

LDMs are celebrated for their ability to produce high-quality outputs with reduced computational demands. By leveraging the efficiencies of latent space, LDMs offer a powerful solution for generating complex data, such as high-resolution images or intricate text sequences, making them a valuable tool in the arsenal of generative modeling techniques. A particular instance of LDMs, a text-to-image DM called Stable Diffusion (<https://github.com/CompVis/stable-diffusion>) has gained unprecedented popularity for its effectiveness in image generation and manipulation.

2.7 Accelerated Sampling Schemes

The iterative nature of physics-inspired GMs is a double-edge sword. On the one hand, it allows for a flexible trade-off between compute and image quality, in addition to zero-shot inverse problem solving. On the other hand, this means that the number of function evaluations (NFE) required may be order of magnitudes larger than for single-step samplers. This computationally heavy sampling limit their usage in applications where speed is of the essence.

One line of work to accelerate sampling involves developing more efficient samplers. In particular, a salient trend is to move from stochastic to deterministic samplers. This was done for DDPMs in Denoising Diffusion Implicit Models (DDIMs) [85] and for SDMs in Karras et al. [54]. Notably, relatively newer methods such as PFGMs [113] and PFGM++ [114] also follow this trend, focusing directly on the ODE instead of the SDE.

Another prominent development in the quest for more efficient sampling are consistency models [90, 86]. Consistency models are a class of GMs that build on the continuous-time formulation of DMs [89, 54] to enable single-step, NFE = 1, sampling. These models achieve this by directly mapping noise to data, enabling high-quality sample generation in a single step, by enforcing self consistency at training time. An illustration of the mapping learned in consistency models is available in Figure 2 (d). Let \mathbf{x}_{σ} denote an intermediate step on the solution trajectory $\{\mathbf{x}_{\sigma}\}_{\sigma \in [\sigma_{\min}, \sigma_{\max}]}$, where $\mathbf{x}_{\sigma_{\min}} \sim p(\mathbf{x})$ and $\mathbf{x}_{\sigma_{\max}} \sim \mathcal{N}(\mathbf{0}, \sigma_{\max}^2)$. Consistency models then strive to learn a consistency function

$$f(\mathbf{x}_{\sigma}, \sigma) \mapsto \mathbf{x}_{\sigma_{\min}} \quad (16)$$

by enforcing self-consistency

$$f(\mathbf{x}_{\sigma}, \sigma) = f(\mathbf{x}_{\sigma'}, \sigma'), \forall \sigma, \sigma' \in [\sigma_{\min}, \sigma_{\max}]. \quad (17)$$

One can ensure that the desired solution is the consistency function in Equation (16) by enforcing the boundary condition

$$f_{\theta}(\mathbf{x}, \sigma) = c_{\text{skip}}(\sigma)\mathbf{x} + c_{\text{out}}(\sigma)F_{\theta}(\mathbf{x}, \sigma), \quad (18)$$

where $c_{\text{skip}}(\sigma)$ and $c_{\text{out}}(\sigma)$ are differentiable functions such that $c_{\text{skip}}(\epsilon) = 1$ and $c_{\text{out}}(\epsilon) = 0$ and $f_{\theta}(\mathbf{x}, \sigma)$ denotes our approximated consistency function via the deep neural network $F_{\theta}(\mathbf{x}, t)$. The domain $[\sigma_{\min}, \sigma_{\max}]$ is discretized using a sequence of noise scales $\sigma_{\min} = \sigma_1 < \sigma_2 < \dots < \sigma_N = \sigma_{\max}$. Following Karras et al. [54], Song et al. [90] set $\sigma_i = (\sigma_{\min}^{1/\rho} + \frac{i-1}{N-1}(\sigma_{\max}^{1/\rho} - \sigma_{\min}^{1/\rho}))^{\rho}$ with $\rho = 7$ for $i = 1, \dots, N$.

Consistency models are trained via the consistency matching loss

$$\mathbb{E} [\lambda(\sigma_i) d(f_{\theta}(\mathbf{x}_{\sigma_{i+1}}, \sigma_{i+1}), f_{\theta^{-}}(\tilde{\mathbf{x}}_{\sigma_i}, \sigma_i))], \quad (19)$$

where

$$\tilde{\mathbf{x}}_{\sigma_i} = \mathbf{x}_{\sigma_{i+1}} - (\sigma_i - \sigma_{i+1})\sigma_{i+1} \nabla_{\mathbf{x}} \log p_{\sigma_{i+1}}(\mathbf{x})|_{\mathbf{x}=\mathbf{x}_{\sigma_{i+1}}}, \quad (20)$$

denotes a single-step in the reverse direction of the PF ODE in Equation (8), $d(\cdot, \cdot)$ a metric function, and $\lambda(\cdot) \in \mathbb{R}_{+}$ a positive weighting function. The expectation in Equation (19) is taken with respect to $i \sim \mathcal{U}[1, N-1]$, a uniform distribution over integers $i = 1, \dots, N-1$, and $\mathbf{x}_{\sigma_{i+1}} \sim p_{\sigma_{i+1}}(\mathbf{x})$. The objective in Equation (19) is minimized via stochastic gradient descent on parameters θ whilst θ^{-} are updated via the exponential moving average (EMA)

$$\theta^{-} \leftarrow \text{stopgrad}(\mu\theta^{-} + (1 - \mu)\theta), \quad (21)$$

where $0 \leq \mu \leq 1$ is the decay rate. Since $\nabla_{\mathbf{x}} \log p_{\sigma_{i+1}}(\mathbf{x})$ is not known, minimizing the objective in Equation (19) is not feasible. Consistency training and consistency distillation are two algorithms to address this issue [90]. Both approaches use an approximation to generate a pair of adjacent points on the solution trajectory, approximately adhering

to Equation (20). Consistency distillation, as the name implies, distills a pre-trained DM into a consistency model and simply replacing the score-function in Equation (20) by a pre-trained score network. Consistency training, on the other hand, is a stand-alone model and estimates the two adjacent points on the solution trajectory via the perturbation kernel. In particular, consistency training obtains the pair of adjacent points on the same solution trajectory $(\mathbf{x}_{\sigma_{i+1}}, \check{\mathbf{x}}_{\sigma_i})$ via $\mathbf{x}_{\sigma_{i+1}} = \mathbf{x} + \sigma_{i+1}\mathbf{z}$ and $\check{\mathbf{x}}_{\sigma_i} = \mathbf{x} + \sigma_i\mathbf{z}$ using the same \mathbf{x} and \mathbf{z} . Consistency training then employ the loss

$$\mathbb{E} [\lambda(\sigma_i) d(f_{\theta}(\mathbf{x} + \sigma_{i+1}\mathbf{z}, \sigma_{i+1}), f_{\theta}(\mathbf{x} + \sigma_i\mathbf{z}, \sigma_i))], \quad (22)$$

which is equivalent to the consistency matching loss in Equation (19) in the $N \rightarrow \infty$ limit [90]. After approximating the consistency function, generating a sample involves sampling an initial noise vector from the noise distribution and applying the consistency model: $\hat{\mathbf{x}} = f_{\theta}(\mathbf{z}, \sigma_{\max})$. Importantly, consistency models maintain the flexibility of balancing image quality against computational efficiency and enable zero-shot data editing, supporting the option of multi-step sampling processes for enhanced control over output quality [90].

Using self-consistency to achieve high fidelity output with significantly less compute has been extended to the case of LDM in Luo et al. [71], with a method called Latent Consistency Distillation (LCD). In addition to generalizing the consistency matching framework to text-to-image LDM, the authors also generalizes the idea of enforcing consistency between adjacent time steps t_{n+1} and t_n to consistency between time steps that are k steps apart, that is t_{n+k} and t_n . This methodology generates impressive state of the art few-step, NFE < 8, text-to-image generation.

Consistency trajectory models (CTMs) [57] learn to estimate both the integrand (the score function) and the integral over any time horizon of the PF ODE, providing a unifying framework which includes consistency models and DMs as special cases. This setup enables anytime-to-anytime jumps, which is leveraged efficiently to trade off compute for image quality via novel sample techniques. In particular, CTMs achieve impressive state of the art performance for unconditional image generation on CIFAR-10 and ImageNet at 64×64 resolution datasets with NFE = 1. Notably, however, CTMs are using a combination of a distillation loss, DSM loss, and an adversarial loss. The inclusion of an adversarial loss can lead to training instability, tentatively negating a key advantage of DMs over GANs.

3 APPLICATIONS IN MEDICAL IMAGING

The advent of physics-inspired GMs has offered new and exciting opportunities in medical imaging. By leveraging the physical principles, these models offer transformative potential in enhancing the performance of medical imaging tasks. In medical imaging, high-quality images are paramount for diagnosis, therapy, and follow-up. Deep GMs, described in Section 2 excel in learning complex data priors, leveraging them to infer missing or corrupted information and generate high-fidelity images. This section delves into three primary applications: I) Image Reconstruction, II) Image Generation, and III) Image Analysis.

3.1 Image Reconstruction

Major medical imaging modalities include CT, MRI, nuclear imaging (PET/SPECT), ultrasound, and optical imaging. The imaging challenges are modality-dependent, such as the radiation dose reduction in CT or the k-space measurement acceleration in MRI, both of which need to handle partial and/or noisy data for tomographic reconstruction.

The raw data acquisition in medical imaging can be modeled by an operator $\mathcal{F} \in \mathbb{R}^n \mapsto \mathbb{R}^m$ acting on the continuous image domain $\mathbf{x} \in \mathbb{R}^n$, resulting in a dataset in the measurement domain $\mathbf{y} \in \mathbb{R}^m = \mathcal{F}(\mathbf{x}) + \mathbf{n}$, where $\mathbf{n} \in \mathbb{R}^m$ represents noise. In CT or PET, \mathcal{F} corresponds to the Radon transform, which produces line integrals of an underlying image to be reconstructed. In SPECT, an attenuated Radon transform is involved. In MRI, \mathcal{F} commonly corresponds to a multi-coil Fourier sampling operator. In practice, the problem is commonly discretized as $\mathbf{y} = \mathbf{A}\mathbf{x} + \mathbf{n}$, where $\mathbf{A} \in \mathbb{R}^{m \times n}$.

The \mathbf{A} can be ill-posed ($m < n$), especially when measurements are taken at sub-Nyquist rates, making direct recovery of \mathbf{x} rather challenging. Taking CT and MRI as two examples, Figure 3 visualizes the measurement techniques used in three specific imaging modes: limited-angle CT (LA-CT), sparse-view CT (SV-CT), and compressed sensing MRI (CS-MRI).

Compressed sensing theory [12, 30] provides a robust foundation for improving sparse-view and low-dose CT reconstruction. Similarly, SENSE (Sensitivity Encoding) [74] is widely used for MRI reconstruction. In a nutshell, compressed sensing-based iterative reconstruction (IR) can be formulated as the optimization problem,

$$\hat{\mathbf{x}} = \arg \min_{\mathbf{x}} \|\mathbf{A}\mathbf{x} - \mathbf{y}\|_2^2 + \lambda \mathcal{R}(\mathbf{x}), \quad (23)$$

where the first term ensures data consistency while $\mathcal{R}(\mathbf{x})$ is a regularization term promoting sparsity, and λ is a regularization parameter. Techniques such as total variation (TV) [115], anisotropic TV [21], total generalized variation (TGV) [73], fractional order TV [120] and many other variants, have all improved reconstruction results.

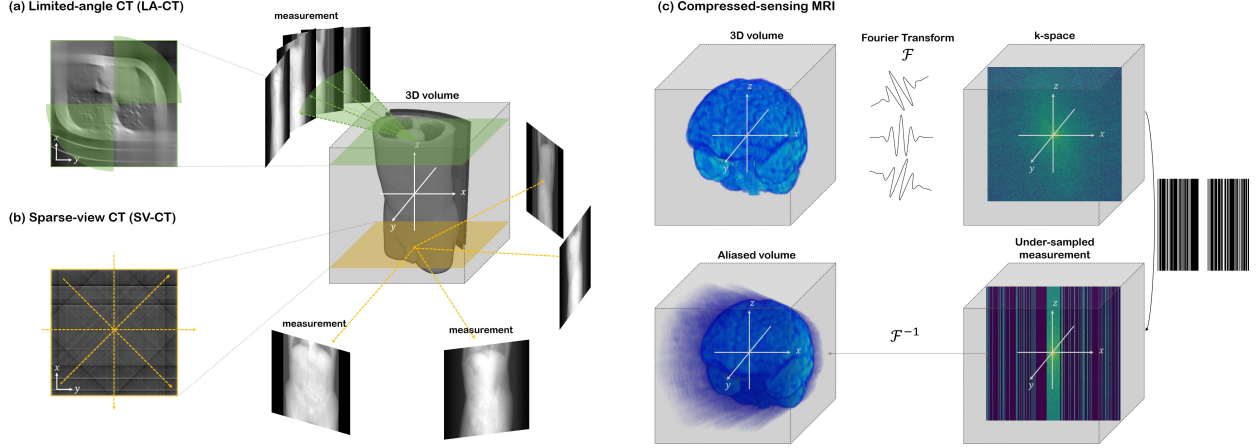


Figure 3: Visualization of three exemplary measurement processes for CT and MRI. (a) limited-angle CT (LA-CT); (b) sparse-view CT (SV-CT); and (c) compressed sensing-based MRI (CS-MRI). Adapted from [26].

Equation (23) is often minimized using iterative first-order optimization algorithms like gradient descent. Starting from \mathbf{x}_0 with a step size η_t , the $(t + 1)^{\text{th}}$ iteration of gradient descent is written as,

$$\mathbf{x}_{t+1} = \mathbf{x}_t - \eta_t \nabla \mathcal{L}(\mathbf{x}_t) = \mathbf{x}_t - \eta_t (\mathbf{A}^T (\mathbf{A} \mathbf{x}_t - \mathbf{y}) + \nabla \mathcal{R}(\mathbf{x}_t)), \quad (24)$$

where $\nabla \mathcal{R}(\mathbf{x}) = \nabla \log p(\mathbf{x})$ represents the score of the distribution, acting as a noise/artifact estimate. Subtracting this term helps refine the image, thus the gradient descent step effectively removes noise and/or aliasing components from the current estimate \mathbf{x}_t .

Traditional image reconstruction methods have been extensively used, such as filtered backprojection (FBP) [1] and iterative reconstruction techniques like the algebraic reconstruction technique (ART) [38], simultaneous algebraic reconstruction technique (SART) [3], and expectation maximization (EM) [29]. However, these methods face limitations due to noise sensitivity, imperfect data challenges, and computational overhead. For example, in sparse-view CT the angular down-sampling fails to satisfy Nyquist’s criterion [108], leading to unsatisfactory results with either analytical or compressed sensing-based iterative reconstruction algorithms, if the down-sampling is done too aggressively.

Deep learning methods for CT image reconstruction have commonly employed supervised learning to map partial measurements to complete images [103, 72], relying on extensive datasets of paired CT images and measurements. However, variations in the measurement process, such as changing CT projections, require new data collection and model retraining. This limits generalization and can sometimes lead to counter-intuitive instabilities [5]. Recently, DMs have addressed these issues by introducing unsupervised training, which provides effective priors without the need for labeled data [88, 22]. These models, which train on high-quality images/data to fill in gaps in down-sampled data, eliminating the need for matched datasets, supporting unsupervised learning and improving tomographic reconstruction quality. The following sub-sections delve into the application of DMs in tomographic, MRI, and PET reconstruction, emphasizing their role in producing superior images and diagnostic performance.

3.1.1 CT Reconstruction

The initial work reported in [88] adapted the diffusion model to medical image reconstruction. This score-based generative model, as outlined in Section 2.3, involves solving inverse problems by generating samples from the posterior distribution $p(\mathbf{x} | \mathbf{y})$. This is achieved by conditioning a stochastic process $\{\mathbf{x}_t\}_{t \in [0,1]}$ on an observation \mathbf{y} , leading to the conditional process $\{\mathbf{x}_t | \mathbf{y}\}_{t \in [0,1]}$. The core of this approach is the conditional stochastic process as a reverse-time SDE:

$$d\mathbf{x}_t = [f(t)\mathbf{x}_t - g(t)^2 \nabla_{\mathbf{x}_t} \log p_t(\mathbf{x}_t | \mathbf{y})] dt + g(t) d\bar{\mathbf{w}}_t, \quad (25)$$

where the conditional score function $\nabla_{\mathbf{x}_t} \log p_t(\mathbf{x}_t | \mathbf{y})$ is approximated with an unconditionally trained score model $s_{\theta^*}(\mathbf{x}, t)$ and the measurement distribution $p(\mathbf{y} | \mathbf{x})$. Notably, this is an unsupervised method and thus does not require paired data.

The method utilizes a special formulation of the linear operator \mathbf{A} , decomposed as $\mathbf{A} = \mathcal{P}(\mathbf{\Lambda})\mathbf{T}$, where \mathbf{T} represents common transforms like Radon, and $\mathbf{\Lambda}$ is a diagonal matrix indicating subsampling. This decomposition facilitates efficient sample generation from $\{\mathbf{x}_t | \mathbf{y}\}_{t \in [0,1]}$ by leveraging an unconditional score model and incorporating the

conditional information. The iterative sampling process modifies existing sampling algorithms by introducing a step that enforces consistency with the observation \mathbf{y} . This is done by solving a proximal optimization problem:

$$\hat{\mathbf{x}}'_{t_i} = \arg \min_{\mathbf{z}} \{(1 - \lambda) \|\mathbf{z} - \hat{\mathbf{x}}_{t_i}\|_{\mathbf{T}}^2 + \min_{\mathbf{u}} \lambda \|\mathbf{z} - \mathbf{u}\|_{\mathbf{T}}^2\}, \quad \text{s.t. } \mathbf{A}\mathbf{u} = \hat{\mathbf{y}}_{t_i}, \quad (26)$$

where λ balances between fitting the sample to both the score model and the observation. The process allows the method to be widely applicable to various sampling methods for various medical image reconstruction tasks. In this study, the norm $\|\mathbf{a}_{\mathbf{T}}^2\| = \|\mathbf{T}\mathbf{a}_2^2\|$ is chosen to simplify the analysis. The decomposition allows for a closed-form solution given by

$$\hat{\mathbf{x}}'_{t_i} = \mathbf{T}^{-1}[\lambda\mathbf{\Lambda}\mathcal{P}^{-1}(\mathbf{\Lambda})\hat{\mathbf{y}}_{t_i} + (1 - \lambda)\mathbf{\Lambda}\mathbf{T}\hat{\mathbf{x}}_{t_i} + (\mathbf{I} - \mathbf{\Lambda})\mathbf{T}\hat{\mathbf{x}}_{t_i}] \quad (27)$$

where $\mathcal{P}^{-1}(\mathbf{\Lambda})$ is a right inverse that increases the dimensionality of a vector by padding entries according to a subsampling mask $\mathbf{\Lambda}$. When $\lambda = 0$, the constraint $\mathbf{A}\hat{\mathbf{x}}'_{t_i} = \hat{\mathbf{y}}_{t_i}$ is ignored, leading to unconditional generation. When $\lambda = 1$, the constraint is exactly satisfied. For noisy measurements, $0 < \lambda < 1$ balances between fitting the data and the constraint.

Along this direction, Cong et al. [27] improved the diffusion model-based tomographic reconstruction approach to perform the MAP reconstruction in the Bayesian framework utilizing a Gaussian mixture model that more accurately captures discrepancies between the distributions of reconstructed images and real counterparts, respectively. This integration facilitates the derivation of a novel score-matching formula implemented via deep learning. The performance of this Gaussian mixture score-matching method was evaluated on both public medical image datasets and clinical raw CT datasets, demonstrating its effectiveness and robustness compared with traditional methods [94] and existing DMs.

While traditional approaches to transmission tomography often rely on linearizing the reconstruction problem, leading to inaccuracies with complex issues, Li et al. [62] introduced a nonlinear method called Diffusion Posterior Sampling (DPS). This method performs CT image reconstruction by integrating a score-based diffusion model with a nonlinear physics-driven measurement likelihood. The DPS method transforms the reconstruction process by applying the Bayesian rule to merge a pre-trained diffusion prior with the gradient of a log-likelihood from a nonlinear model into a posterior score function described as follows:

$$\nabla_{\mathbf{x}_0} \log p(\mathbf{y}|\mathbf{x}_0) = -\mathbf{A}^T \mathbf{y} + \mathbf{A}^T D\{I_0 \exp(-\mathbf{A}\mathbf{x}_0)\}, \quad (28)$$

where $\{\cdot\}^T$ denotes a matrix transpose, and \mathbf{A}^T represents backprojection. This adaptation aligns the reconstructed images with the actual nonlinear measurements with the CT system. Efficiency in reconstruction is enhanced through a heuristic weighting scheduler. The process is further streamlined by an ordered-subset approach, leading to the order-subset DPS nonlinear (OS-DPS Nonlinear) algorithm. This innovative approach has proven both effective and efficient over existing deep learning methods.

As an example of accelerating techniques in DMs for alleviating computational burdens, discussed in Section 2.7, Liu et al. [66] have adopted a Fourier diffusion approach originally from [96]. This method considerably cuts down the number of required time steps compared to traditional scalar DMs. Specifically tailored for X-ray transmission tomography and FBP processes, their technique efficiently estimates image properties in sparse CT systems. They validated the efficacy of this approach by demonstrating its ability to maintain image quality while reducing computational demands in a simulated breast cone-beam CT system with sparse view acquisition.

Beyond the mentioned techniques for CT reconstruction, emerging implicit neural representation (INR) methods have shown promise in addressing underdetermined CT reconstruction tasks [118, 75, 107]. However, the unsupervised nature of INR architectures offers limited constraints on the solution space, posing challenges in highly ill-posed scenarios like LA-CT and ultra sparse-view computed tomography (ultraSVCT). To bridge this gap, Du et al. [31] developed a hybrid network known as the Diffusion Prior Driven Neural Representation (DPER). This framework integrates a score-based diffusion model with INR optimization, employing the half quadratic splitting (HQS) [36] algorithm to enhance data fidelity. DPER leverages both the image acquisition model based on physics and the continuity prior from INR, resulting in accurate and stable CT image reconstructions. This approach delivered a superior performance on the AAPM and LIDC [6] datasets, compared to SCOPE [107] and DiffusionMBIR [26].

To further alleviate the computational bottleneck in DDPMs, as investigated in Section 2.1, the patch-based DDPM, [108] was designed so that the diffusion-based inverse problem can be solved in a distributed parallel fashion. This novel approach was demonstrated for sparse-view CT reconstruction. The network, trained on patches from fully sampled projection data, enables unsupervised inpainting of down-sampled data without the need for paired datasets. By employing a patch-based approach, this method allows for distributed parallel processing, mitigating memory issues. Additionally, a projection-domain patch-based DDPM method is inspired by using a U-Net [77] to learn the reverse diffusion process on fully sampled projection patches. The reconstructed patches are finally assembled to form a high-quality projection dataset for FBP image reconstruction, Such an integration of unsupervised learning and

parallel computing capability makes the diffusion model suitable for large-scale tasks. Indeed, Xia et al. [109] further refined the approach for breast CT reconstruction, which uses parallel DDPM in both image and sinogram domains for sparse-view reconstruction, significantly reducing radiation doses while maintaining competitive results.

Using PFGM, as detailed in Section 2.4, Ge et al. [35] introduced the Joint Condition and Circle-Supervision algorithm for multiphase contrast-enhanced CT (CECT), optimizing image quality across various imaging phases. This strategy integrates temporal progression and spatial correlations to reduce the involved radiation dose. To further enhancement of this approach, as outlined in Section 2.5, Hein et al. [46] presented a PFGM++ approach to photon-counting CT (PCCT) image denoising via posterior sampling. Their strategy employs a consistency-enforced sampling scheme, using a ‘hijacking’ technique that integrates noisy observations directly into the reverse generative process [84, 24, 69]. This avoids complex regularization, effectively approximating the true image from noisy data [55]. Hein et al. [47] further developed this framework with the Posterior Sampling Poisson Flow Consistency Model (PS-PFCM), which optimizes computational efficiency, leveraging a “consistency distillation” process and enabling single-step or few-step function evaluations [91].

3.1.2 MRI Reconstruction

Similar to deep CT image reconstruction, deep MRI image reconstruction can be viewed in two categories: model-driven and data-driven methods [37], although there are not clear boundary between these methods. Model-driven methods rely on mathematically derived optimization equations and incorporate artificial neural networks (ANNs) to enhance accuracy and efficiency [80]. Data-driven methods extract patterns and correlations from large datasets using advanced deep learning techniques in an end-to-end fashion [7]. Both methods can improve MRI reconstruction, balancing accuracy, efficiency, and robustness in different ways.

Chung et al. [25] combine the Krylov subspace method [64] with the diffusion model for complex imaging tasks, such as multi-coil MRI and 3D CT scans. This method, called Decomposed Diffusion Sampling (DDS), uses the fast-converging traits of the Krylov subspace method, known from traditional optimization studies, together with the strong generation abilities of the contemporary DMs. The key to DDS is its use of the manifold constrained gradient (MCG) [23]. DDS shows that the tangent space at a cleaned-up sample, according to Tweedie’s formula, matches a Krylov subspace. This insight allows the method to perform multiple conjugate gradient (CG) updates within this space, simplifying the process significantly. Mathematically, this process is expressed as

$$\hat{\mathbf{x}}'_t = \text{CG}(\mathbf{A}^* \mathbf{A}, \mathbf{A}^* \mathbf{y}, \hat{\mathbf{x}}_t). \quad (29)$$

Then, the DDS algorithm is defined as

$$\mathbf{x}_{t-1} = \sqrt{\tilde{\alpha}_{t-1}} \hat{\mathbf{x}}'_t + \tilde{\mathbf{w}}_t, \quad \hat{\mathbf{x}}'_t = \text{CG}(\mathbf{A}^* \mathbf{A}, \mathbf{A}^* \mathbf{y}, \hat{\mathbf{x}}_t, M), \quad M \leq l, \quad (30)$$

where $\tilde{\mathbf{w}}_t$ is the noise element, and M is the number of the CG steps within the Krylov subspace.

Chung et al. [26] introduced DiffusionMBIR, a novel method that combines model-based iterative reconstruction (MBIR) with 2D diffusion modeling to meet the 3D image reconstruction challenges like sparse-view tomography and compressed sensing MRI. This approach marries the precision of MBIR with the generative power of the diffusion model, enabling efficient, high-fidelity reconstructions on a single commodity GPU. The innovation of DiffusionMBIR lies in augmenting a 2D diffusion prior with a model-based TV prior, applied specifically in the longitudinal direction at test time. This method uses the alternating direction method of multipliers (ADMM) [11] to integrate measurement information and enforce consistency across slices:

$$\begin{aligned} \mathbf{x}^+ &= \underbrace{(\mathbf{A}^T \mathbf{A} + \rho \mathbf{D}_z^T \mathbf{D}_z)}_{\mathbf{A}_{\text{CG}}}^{-1} \underbrace{(\mathbf{A}^T \mathbf{y} + \rho \mathbf{D}^T (\mathbf{z} - \mathbf{w}))}_{\mathbf{b}_{\text{CG}}}, \\ \mathbf{z}^+ &= S_{\lambda/\rho}(\mathbf{D}_z \mathbf{x}^+ + \mathbf{w}), \quad \mathbf{w}^+ = \mathbf{w} + \mathbf{D}_z \mathbf{x}^+ - \mathbf{z}^+. \end{aligned} \quad (31)$$

where ADMM updates apply soft-thresholding to the gradient of the image reconstruction ($\mathbf{D}_z \mathbf{x}^+$) and adjust the dual variable (\mathbf{w}), promoting sparsity and ensuring consistency across the z -direction and accommodating image cubes 256^3 or greater.

He et al. [44] also addressed high resource consumption and difficulties in capturing a natural distribution of 3D medical images, which is referred to as Blaze3DM. This method integrates compact triplane neural fields with a powerful diffusion model for MRI reconstruction. The method begins by optimizing data-dependent triplane embeddings and a shared decoder simultaneously to reconstruct each triplane back to the corresponding 3D volume. A lightweight 3D-aware module is used to extract the correlation among three planes. Then, a diffusion model, trained on latent triplane embeddings, achieves both unconditional and conditional triplane generation.

During sampling, the diffusion model can be guided by degradation constraints to generate arbitrary-sized 3D volumes. Experiments demonstrate that Blaze3DM achieves the state-of-the-art performance and improves computational efficiency compared to existing 3D medical inverse problem solvers, including compressed-sensing MRI, DiffusionM-BIR [26] and TPDM [61].

To further enhance MRI quality, Geng et al. [37] introduced a comprehensive detail-preserving method using multiple DMs to extract structural and textural features in the k-space. Traditional DMs often struggle with capturing intricate details accurately [79, 42]. The proposed method employs virtual binary modal masks to refine the value range of k-space data, which places the model focus within a highly adaptive center window. An inverted pyramid structure is used, allowing for a multi-scale representation. Empirically, a step-by-step refinement significantly enhances detailed image features on the selected benchmark datasets.

Similarly, Guan et al. [40] proposed another MRI reconstruction scheme that leverages k-space data properties and the diffusion process to enhance image quality. By mining multi-frequency priors using diverse strategies, the proposed method preserves image texture and accelerates the sampling process. A key to this method is the Correlated and Multi-frequency Diffusion Modeling (CM-DM), which combines the *Weight-K-Space* and *Mask-K-Space* strategies to optimize the utilization of hidden information. This scheme outperforms the state-of-the-art methods in maintaining image details, not only improving reconstruction accuracy but also facilitating fast convergence by focusing on high-frequency priors.

3.1.3 Nuclear Imaging

In the previous sub-sections, we comprehensively discussed the applications of physics-inspired generative models in CT and MRI reconstruction tasks. In this sub-section, we want to show that physics-informed generative models can be also utilized for other imaging modalities with an emphasis on PET image reconstruction.

PET image reconstruction faces challenges such as high variance Poisson noise and a wide dynamic range. To address these issues, Singh et al. [82] proposed PET-specific score-based generative models, including a framework for both 2D and 3D PET and an extension for guided reconstruction using MRI images. Validated through experiments on patient-realistic data, the proposed method demonstrates robust results with potential for improving PET reconstruction quality.

As another innovative approach for PET imaging, Chen et al. [18] introduced the 2.5D Multi-view Averaging Diffusion Model (MADM). This model converts non-attenuation-corrected low-dose PET (NAC-LDPET) into attenuation-corrected standard-dose PET (AC-SDPET), lowering the tracer dose and eliminating the need for CT-based attenuation correction. MADM uses separate DMs for axial, coronal, and sagittal views, averaging outputs to produce high-quality 3D images. The 2.5D architecture reduces computational demands and mitigates 2D discontinuities. In their experiments, MADM outperformed the competitive methods, offering high-quality 3D PET images with reduced radiation exposure and improved computational efficiency.

To further address the challenges of generalizability across different image noise levels, acquisition protocols, and patient populations in low-dose PET imaging, Xie et al. [110] developed DDPET-3D, a dose-aware diffusion model specifically for 3D low-dose PET imaging. Traditional DMs struggled with consistent 3D reconstructions and generalization across varying noise levels, often resulting in visually appealing but distorted images. DDPET-3D was extensively evaluated using 9,783 F-FDG studies from 1,596 patients across four medical centers with different scanners and clinical protocols. The model demonstrated strong generalizability to different low-dose levels, scanners, and protocols. Reader studies by nuclear medicine physicians confirmed that DDPET-3D produced superior denoised results comparable to or better than 100% full-count images and previous deep learning baselines. Real low-dose scans were included to showcase the clinical potential of DDPET-3D, indicating the feasibility of achieving high-quality low-dose PET images.

Given the limited space of this review, we will not delve into details on the applications of the diffusion model in other imaging modalities such as ultrasound imaging [125, 126], histopathology [92], and endoscopy [19].

3.2 Medical Image Generation

Generating synthetic images through advanced generative models is a crucial area that addresses the scarcity of annotated medical datasets and ethical concerns associated with using real patient data. Techniques based on physics-informed models and their derivatives, explored in Section 2, are particularly effective at producing high-quality, diverse synthetic images that accurately replicate human anatomy and disease variations, providing valuable resources for training algorithms and testing new technologies [51].

3.2.1 High-Quality Image Synthesis

DMs have revolutionized medical image synthesis by addressing dataset scarcity, memory constraints, and computational complexity. These models generate high-quality images realistically, providing essential resources for developing and testing medical imaging algorithms [78].

To address the limited availability of 3D medical image datasets, Zhu et al. [130] developed GEM-3D, a generative approach using conditional DMs to synthesize and enhance 3D medical images. GEM-3D begins with a 2D slice containing patient-specific information and uses a 3D segmentation mask to guide the generation process. By decomposing 3D images into masks and patient prior information, GEM-3D enables versatile image generation, counterfactual synthesis, and dataset enhancement. This approach improves the quality and variability of generated 3D images, tackling high-quality 3D generation and condition decoupling for re-sampling data. The key innovation lies in decomposing segmentation masks and patient information for data augmentation, improving distribution coverage.

Furthermore, Ju and Zhou [53] introduced a hybrid diffusion model based on a State Space Model (SSM). This model combines the local perception capabilities of CNNs with the global attention of SSM, while maintaining linear computational complexity [45]. The architecture features a multi-level feature extraction module called the Multi-level State Space Block (MSSBlock) and an encoder-decoder structure with the State Space Layer (SSLayer), designed specifically for medical pathological images. Additionally, a Sequence Regeneration strategy improves the cross-scan module (CSM), enabling the Mamba [39] module to fully capture image spatial features and enhance model generalization. This hybrid architecture produced a competitive performance, according to a qualitative assessment by radiologists.

To ease the tension between high-dimensional data and limited GPU memory [129], [33] introduced wavelet diffusion models (WDMs), a wavelet-based medical image synthesis framework that applies DMs to wavelet-decomposed images. WDM generates high-resolution 3D medical images by creating synthetic wavelet coefficients and then applying inverse discrete wavelet transform (IDWT). By decomposing an input image into a limited number of wavelet coefficients, concatenated into a single target matrix for the diffusion model, WDM maintains the standard architecture's width through an initial convolution. Operating in the wavelet domain reduces spatial dimensions significantly, allowing for shallower networks, fewer computations, and reduced memory usage. During training, a corrupted sample is drawn, and the diffusion model approximates the original wavelet coefficients in terms of mean squared error. Inference starts with a sample from a normal distribution, and goes through reverse diffusion to reconstruct a final image. In the experiments, WDM outperformed the state-of-the-art methods in high-resolution 3D medical image generation.

In another study, Huang et al. [50] introduced a cascaded amortized latent diffusion model (CA-LDM) to synthesize high-resolution OCT volumes efficiently. This model employs non-holistic auto-encoders (NHAE) to map between low-resolution latent spaces, as mentioned in Section 2.6, and high-resolution volumes, achieving volumetric super-resolution slice-by-slice to manage the memory constraint. Cascaded diffusion processes further enhance this memory efficiency by first synthesizing the 3D global latent representation, followed by a 2D slice-wise refinement for high-resolution details. This approach effectively balances memory and speed in a task-specific way.

Yet another approach to reducing the number of inference steps is Fast-DDPM [52]. This model reduces training and sampling to just 10 time steps, optimizing the process with an appropriate noise scheduler. By aligning training and sampling procedures, Fast-DDPM enhances training speed, sampling speed, and generation quality. Evaluated on important tasks such as multi-image super-resolution, image denoising, and image-to-image translation, Fast-DDPM demonstrated its effectiveness in minimizing computational overhead while maintaining high performance relevant to medical imaging applications.

3.2.2 Image Segmentation and Anatomical Guidance

In medical image generation, leveraging anatomical structures significantly enhances the precision and robustness of synthesized images. This approach targets the inherent complexity and variability of human anatomy, ensuring that generated images are clinically relevant. By incorporating anatomical guidance, these techniques provide major improvements in the fidelity and utility of synthesized medical images, which are essential for training and validating deep imaging algorithms.

To further enhance medical image generation, Konz et al. [59] proposed SegGuidedDiff, a diffusion model using multi-class anatomical segmentation masks at each sampling step. This method incorporates a random mask ablation training stage, allowing the model to condition on specific anatomical constraints while maintaining flexibility. SegGuidedDiff generates images directly from anatomical segmentation maps, ensuring precise spatial guidance. The evaluative studies on breast MRI and abdominal/neck-to-pelvis CT datasets demonstrated that SegGuidedDiff achieved excellent performance, producing realistic images faithful to the input masks.

Similarly, LeFusion, a lesion-focused diffusion model [121], addresses long-tail imbalance and algorithmic unfairness in clinical data by focusing on lesion areas [15]. Inspired by diffusion-based inpainting, LeFusion integrates the background context into the reverse diffusion process, preserving background quality while handling multi-class lesions flexibly. This method diversifies image synthesis by introducing lesion masks. On the DE-MRI cardiac lesion segmentation dataset (Emidec) [60], LeFusion significantly outperformed the nnUNet model’s performance.

3.2.3 Data Imbalance and Image Robustness

Addressing data imbalance and enhancing model robustness are critical in medical image generation. These issues often induce biases and reduce generalizability.

Chambon et al. [14] introduced a vision-language foundation model called RoentGen to generate synthetic chest X-rays (CXR) based on text prompts. It leverages a pre-trained LDM fine-tuned on publicly available CXRs and radiology reports for the creation of diverse, high-quality images guided by radiology-specific text prompts. This method enhances image classification tasks through data augmentation. RoentGen’s architecture includes a VAE, a conditional denoising U-Net, and a CLIP text encoder. The U-Net and text encoder are fine-tuned on the MIMIC-CXR dataset while the VAE is kept frozen. The model samples noise from a Gaussian distribution and predicts the original noise using the U-Net and encoded text prompts.

Another contribution to this field is Cheff, a cascaded latent diffusion model introduced by Weber et al. [102]. Cheff generates highly realistic 1-megapixel chest radiographs and addresses class imbalances by leveraging “MaCheX”, the largest open collection of chest X-ray datasets, which supports report-to-chest-X-ray generation [93]. This methodology integrates auto-encoders and super-resolution DMs, setting a new standard in radiological image synthesis.

Additionally, the MedM2G framework [119] presents a unified approach for medical multi-modal generation. MedM2G overcomes the limitations of separate generative models by aligning and generating medical data across multiple modalities (CT, MRI, X-ray) within a single model. It makes a central alignment to integrate diverse medical datasets, preserves specific clinical knowledge through visual invariability, and enhances cross-modal interactions using adaptive diffusion parameters. MedM2G outperforms the state-of-the-art models in the relevant tasks including text-to-image and image-to-text generation, in terms of accuracy and efficiency across multiple medical datasets.

3.2.4 Innovative Frameworks for Image Generation

Developing innovative frameworks for generative AI is essential for advancing the quality and utility of synthetic images. This includes methodologies for inpainting, counterfactual generation, and multi-modal alignment, which will be instrumental in meeting several medical imaging challenges.

The Concept Discovery through Latent diffusion-based counterfactual trajectories (CDCT) framework [97] addresses classifier biases and uncovers medical concepts by using LDMs to generate counterfactual trajectories. This approach involves generating trajectories with LDMs, disentangling semantic spaces with a VAE, and identifying relevant concepts through a search algorithm. This method significantly improves high-fidelity, patient-specific 3D medical image generation.

Another novel technique utilizes voxel-wise noise scheduling in LDM for inpainting pathological features into lumbar spine MRIs [43]. This method overcomes the limitations of traditional data augmentation models by ensuring better anatomical integration, significantly improving the results of lumbar spine MRI.

3.3 Medical Image Analysis

In medical image analysis, innovative techniques are continually emerging in various clinical tasks. Recent advancements in texture restoration [99, 101, 112], denoising [46, 111], anomaly detection [34, 81, 32, 9], and segmentation [17, 106, 122, 10] have significantly improved the quality of medical images, suggesting a great potential of contemporary AI generative models. A few representative examples are as follows.

Wang et al. [101] introduced the implicit image-to-image Schrödinger bridge (I^3SB), an enhanced version of the Image-to-Image Schrödinger Bridge (I^2SB) [67]. I^3SB employs a non-Markovian process that integrates corrupted images at each generative step, significantly improving texture restoration and accelerating generation, particularly in CT super-resolution and denoising tasks. By establishing a diffusion bridge between clean and corrupted images, I^3SB optimizes generative steps to produce high-quality images. This method outperformed traditional models like cDDPM on the RPLHR-CT-tiny [117] datasets.

Chen et al. [16] designed the Bernoulli Diffusion model for medical image segmentation (BerDiff), which improves traditional diffusion methods by incorporating Bernoulli noise, making it better suited for binary segmentation tasks [2,

[105]. This approach generates more accurate and diverse segmentation masks, crucial for delineating ambiguous tumor boundaries. BerDiff provides multiple plausible segmentation options by sampling different initial noises and intermediate states. Evaluated on various medical imaging datasets, BerDiff outperformed the current methods, showcasing its potential for clinical imaging tasks [104].

To shorten prediction time of the diffusion model, Zhang et al. [122] presented CTS, a consistency-based medical image segmentation model, as noted in Section 2.7. By condensing sampling into a single iteration, CTS accelerates training and prediction while maintaining the generation quality [91]. This model uses multi-scale feature supervision and customized loss functions to improve segmentation and convergence. It integrates multi-scale signals into the UNet model and iteratively refines parameters, capitalizing contextual information.

In response to the limitations of 2D methods, which often miss crucial out-of-slice information, Kim and Park [58] introduced a refined LDM with a novel switchable block, the multiple switchable spatially adaptive normalization (MS-SPADE). This innovation enables effective 3D medical image translation without patch cropping, allowing for the translation of multiple target modalities from a single source. The MS-SPADE block dynamically adjusts source latents to match target styles, improving fidelity and reducing the need for multiple models, thereby addressing practical challenges like high scan costs and limited availability in clinical settings.

Furthermore, Arslan et al. [8] address key challenges in DDMs used for medical image translation, particularly the weak guidance from source modalities and the poor alignment between denoising and the necessary transformations from source to target that reduce effectiveness [41]. They present the Self-consistent Recursive Diffusion Bridge (SelfRDB). This model markedly better traditional DDMs by introducing a forward process with a strategy that gradually increases noise levels, improving generalization and boosting the transfer of information between modalities. SelfRDB stands out from typical DMs by using a special recursive estimation method in its backward steps, which permits ongoing improvement of the target image while keeping the original tissue details intact. Extensive tests on multi-contrast MRI and MRI-CT translations show that SelfRDB surpasses current GAN [128] and DMs and is the first to employ a soft-prior on the source modality and a consistent recursive estimation to refine the accuracy of backward diffusion steps.

Zheng et al. [127] presented the Deformation-Recovery Diffusion Model (DRDM), a novel approach that shifts from traditional intensity-based synthesis [84] to deformation-based methods [123], using a mechanism that generates topologically-preserving multi-scale Deformation Velocity Fields (DVF). This model enhances the interpretability and anatomical accuracy of synthetic medical images by creating physically plausible deformation fields. Capable of managing instance-specific deformations without reference images, the DRDM supports applications such as data augmentation for few-shot learning and synthetic training for image registration. This advancement enriches synthetic medical image generation and aids critical downstream tasks without the need for external annotations.

Finally, FlowSDF [10] is another image-guided conditional flow matching framework through the signed distance function (SDF), facilitating an implicit distribution of segmentation masks. By leveraging SDF, FlowSDF achieves more natural distortions and high-quality sampling from the segmentation mask distribution of interest, enhancing predictive robustness with statistical tools like uncertainty maps. This method employs ODE-based flow matching [65, 68] to model probability flow, ensuring a smoother distribution and natural transitions between class modes. FlowSDF integrates image-guided flow matching with SDFs, enabling noise-injection for generating multiple segmentation maps and uncertainty quantification, thus improving model robustness and interpretability.

4 FUTURE DIRECTIONS

Physics-inspired GMs excel at closely matching the distribution of real images. This has not only paved the way for various medical imaging applications (as outlined in the previous section), but also offers potential for future developments along several research directions. Since hot topics for DDPMs are comprehensively covered in [56], this section focuses on other types of physics-inspired GMs, as well as more general aspects such as unification of GMs and performance considerations.

4.1 Unification of SDMs

DDPMs (cf. Section 2.1) are grounded on the concept of non-equilibrium thermodynamics, specifically employing a diffusion-like process to progressively shape random noise into coherent data. PFGMs (cf. Section 2.4) are based on electrostatics, where the Poisson equation is used to describe the evolution of particles under the influence of electrostatic force. Accordingly, the question arises whether other physical phenomena can also give rise to GMs, or in other words, whether a duality between a physical phenomenon and a respective “score-matching” GM exists [70]. Liu

et al. [70] show that this can indeed be the case, under several restrictions on the physical processes. This opens up a wide range of new options that take advantage of physical processes for advancing medical imaging research.

4.2 Integration with VLMs

Whilst DMs have shown excellent performance on various image generation tasks (both in medical imaging as detailed in Section 3, as well as various other fields), Large Language Models (LLMs) are dominant for generative tasks in natural language processing (NLP). Nevertheless, if a dedicated visual tokenizer that maps pixel-space inputs to discrete tokens can be effectively analyzed by LLMs, the resultant vision-language models may even outperform DMs on image and video generation benchmarks including ImageNet and Kinetics [116].

Instead of using either a DM or a LLM, an increasing number of research efforts are capitalizing on both types of models synergistically. The canonical way of obtaining VLMs, or more generally multimodal models, would be to combine several models; for example, an image encoder to understand images, an LLM to generate text, and a DM to generate images. A very interesting recent development is Chameleon [95], which represents a new approach of early-fusion token-based mixed-modal models designed to comprehend and produce images and text in any order. The flexibility of such models may prove useful in the field of medical imaging.

Integrating DMs and LLMs offers the following potential benefits. I) Diverse strengths: Each model type excels in a unique aspect; combining them leverages their strengths. II) Complementary information: Language models extract semantic information from text prompts, guiding the DM for more accurate results (e.g. in image generation or image reconstruction). III) Progressive refinement: LLMs provide initial concepts, which may be refined by score-matching models into more realistic images, yielding higher fidelity. IV) Task simplification: Integrating models specializing in different sub-tasks divides and conquers the complexity of tasks, thus enhancing efficiency, which is highly desirable for many challenging medical imaging applications.

However, in spite of recent advancements in text-to-image generation with diffusion or score-matching models, they often struggle to accurately follow the prompts when spatial or common sense reasoning is required [63]. Vice versa, adaptation of LLMs to medical imaging is not straight-forward, since they have safeguards regarding medical imaging data. As a result, performance of proprietary LLMs, such as ChatGPT-4, is usually quite poor for medical image synthesis and thus domain adaptation using task-specific medical datasets is often required.

Therefore, extensive research efforts are under way to explore how to link both models and how to take advantage of the strengths of each model for generative tasks. In this context, there are several studies on different types of GMs. For instance, in [63], a DM for text-to-image scene generation is enhanced with a LLM that generates a scene layout with captioned bounding boxes to handle more complex prompts. In [20] an autoencoder is enhanced with high-level features from a pre-trained LLM and its vocabulary. Regarding PFGMs and PFGM++ (cf. Sections 2.4 and 2.5), their integration with LLMs is largely untouched so far. Therefore, further research is clearly needed.

4.3 Novel Applications of GMs

Physics-inspired GMs have shown great potential in the context of various medical imaging modalities (cf. Section 3.1) and associated tasks (cf. Sections 3.2 and 3.3). It is expected that these models will be adapted to novel imaging modalities, such as phase-contrast and dark-field imaging techniques, spectral imaging, or multi-modal and multi-contrast approaches. Furthermore, generalist DMs are attractive, because these foundation models will be able to simultaneously cover multiple medical image domains and handle diverse clinical tasks. By taking advantage of multiple domains simultaneously, more robust performance on clinical tasks with scarce data is to be expected using the AI generalist approach.

Despite these potentials, there are several limitations regarding the score-matching generative models in medical imaging. Medical image data is always linked with protected health information (PHI), and protecting PHI is a critical aspect that needs to be taken care of. Although some of the proposed DMs could have a large clinical impact in medical imaging and image analysis, in many cases limitations arise due to the lack of data availability limited by the PHI concerns. This is particularly evident in applications such as personalized medicine, rare diseases, longitudinal studies, and multi-institutional collaborations. Moreover, different imaging modalities, varying quality of scans and diverse patient demographics are inherent characteristics of medical image data. Furthermore, insufficient computing resources is an obstacle for DM training when addressing non-trivial datasets, given an extensive computational cost of DMs in general. Memory efficient methods, such as Low-Rank Adaptation (LoRA) [49], offer some democratization of the field by enabling users to adapt DMs to their domain of interest at a lower computational cost. Finally, general theoretical insights regarding score-matching GMs would be generally desirable and particularly in medical imaging areas. Further

theoretical insights and practical solutions are anticipated to address potential biases, instability, hallucination, and sub-optimality in training quality and efficiency.

5 CONCLUSION

In this article, we have provided a general overview of different physics-inspired GMs and associated acceleration techniques. Furthermore, we have highlighted their applications in different medical imaging scenarios, including medical image reconstruction, image generation, and image analysis. Finally, we have discussed future research directions, such as unification of GMs, integration with VLMs, new applications of GMs, including foundation models, as well as challenges to overcome. Clearly, there is immense potential for physics-inspired GMs and great opportunities to solve the current problems and redefine medical imaging.

References

- [1] Marwa Al and Mohammed Al-Hayani. The use of filtered back projection algorithm for reconstruction of tomographic image. pages 151–156, 01 2014.
- [2] Tomer Amit, Tal Shaharbany, Eliya Nachmani, and Lior Wolf. Segdiff: Image segmentation with diffusion probabilistic models, 2022.
- [3] Anders H Andersen and Avinash C Kak. Simultaneous algebraic reconstruction technique (SART): a superior implementation of the ART algorithm. *Ultrasonic imaging*, 6(1):81–94, 1984.
- [4] Brian D.O. Anderson. Reverse-time diffusion equation models. *Stochastic processes and their applications*, 12(3):313–326, 1982. ISSN 0304-4149.
- [5] Vegard Antun, Francesco Renna, Clarice Poon, Ben Adcock, and Anders Hansen. On instabilities of deep learning in image reconstruction - does ai come at a cost?, 02 2019.
- [6] Samuel G Armato III, Geoffrey McLennan, Luc Bidaut, Michael F McNitt-Gray, Charles R Meyer, Anthony P Reeves, Binsheng Zhao, Denise R Aberle, Claudia I Henschke, Eric A Hoffman, et al. The lung image database consortium (lidc) and image database resource initiative (idri): a completed reference database of lung nodules on ct scans. *Medical physics*, 38(2):915–931, 2011.
- [7] Simon Arridge, Peter Maass, Ozan Öktem, and Carola-Bibiane Schönlieb. Solving inverse problems using data-driven models. *Acta Numerica*, 28:1–174, 2019.
- [8] Fuat Arslan, Bilal Kabas, Onat Dalmaz, Muzaffer Ozbey, and Tolga Çukur. Self-consistent recursive diffusion bridge for medical image translation. *arXiv:2405.06789*, 2024.
- [9] Cosmin I. Bercea, Benedikt Wiestler, Daniel Rueckert, and Julia A. Schnabel. Diffusion models with implicit guidance for medical anomaly detection, 2024.
- [10] Lea Bogensperger, Dominik Narnhofer, Alexander Falk, Konrad Schindler, and Thomas Pock. Flowsdf: Flow matching for medical image segmentation using distance transforms, 2024. URL <https://arxiv.org/abs/2405.18087>.
- [11] Stephen Boyd, Neal Parikh, Eric Chu, Borja Peleato, and Jonathan Eckstein. Distributed optimization and statistical learning via the alternating direction method of multipliers. *Foundations and Trends in Machine Learning*, 3:1–122, 01 2011. doi:[10.1561/22000000016](https://doi.org/10.1561/22000000016).
- [12] Emmanuel J Candès, Justin Romberg, and Terence Tao. Robust uncertainty principles: Exact signal reconstruction from highly incomplete frequency information. *IEEE Transactions on information theory*, 52(2):489–509, 2006.
- [13] Hanqun Cao, Cheng Tan, Zhangyang Gao, Yilun Xu, Guangyong Chen, Pheng-Ann Heng, and Stan Z Li. A survey on generative diffusion model. 2023.
- [14] Pierre Chambon, Christian Bluethgen, Jean-Benoit Delbrouck, Rogier Van der Sluijs, Małgorzata Połacin, Juan Manuel Zambrano Chaves, Tanishq Mathew Abraham, Shivanshu Purohit, Curtis P. Langlotz, and Akshay Chaudhari. Roentgen: Vision-language foundation model for chest x-ray generation, 2022.
- [15] Richard J. Chen, Tiffany Y. Chen, Jana Lipkova, Judy J. Wang, Drew F. K. Williamson, Ming Y. Lu, Sharifa Sahai, and Faisal Mahmood. Algorithm fairness in ai for medicine and healthcare, 2022.
- [16] Tao Chen, Chenhui Wang, and Hongming Shan. *BerDiff: Conditional Bernoulli Diffusion Model for Medical Image Segmentation*, page 491–501. Springer Nature Switzerland, 2023. ISBN 9783031439018. doi:[10.1007/978-3-031-43901-8_47](https://doi.org/10.1007/978-3-031-43901-8_47). URL http://dx.doi.org/10.1007/978-3-031-43901-8_47.

- [17] Tao Chen, Chenhui Wang, and Hongming Shan. Berdiff: Conditional bernoulli diffusion model for medical image segmentation. In *International conference on medical image computing and computer-assisted intervention*, pages 491–501. Springer, 2023.
- [18] Tianqi Chen, Jun Hou, Yinchu Zhou, Huidong Xie, Xiongchao Chen, Qiong Liu, Xueqi Guo, Menghua Xia, James S. Duncan, Chi Liu, and Bo Zhou. 2.5d multi-view averaging diffusion model for 3d medical image translation: Application to low-count pet reconstruction with ct-less attenuation correction, 2024. URL <https://arxiv.org/abs/2406.08374>.
- [19] Tong Chen, Qingcheng Lyu, Long Bai, Erjian Guo, Huxin Gao, Xiaoxiao Yang, Hongliang Ren, and Luping Zhou. Lightdiff: Surgical endoscopic image low-light enhancement with t-diffusion, 2024. URL <https://arxiv.org/abs/2405.10550>.
- [20] Zhihao Chen, Tao Chen, Chenhui Wang, Chuang Niu, Ge Wang, and Hongming Shan. Low-dose ct denoising with language-engaged dual-space alignment, 2024.
- [21] Zhiqiang Chen, Xin Jin, Liang Li, and Ge Wang. A limited-angle ct reconstruction method based on anisotropic tv minimization. *Physics in Medicine & Biology*, 58(7):2119–2141, 2013.
- [22] Hyungjin Chung, Jeongsol Kim, Michael T Mccann, Marc L Klasky, and Jong Chul Ye. Diffusion posterior sampling for general noisy inverse problems. *arXiv preprint arXiv:2209.14687*, 2022.
- [23] Hyungjin Chung, Byeongsu Sim, Dohoon Ryu, and Jong Chul Ye. Improving diffusion models for inverse problems using manifold constraints. *Advances in Neural Information Processing Systems*, 35:25683–25696, 2022.
- [24] Hyungjin Chung, Byeongsu Sim, and Jong Chul Ye. Come-closer-diffuse-faster: Accelerating conditional diffusion models for inverse problems through stochastic contraction. In *Proceedings of the IEEE/CVF Conference on Computer Vision and Pattern Recognition*, pages 12413–12422, 2022.
- [25] Hyungjin Chung, Suhyeon Lee, and Jong Chul Ye. Decomposed diffusion sampler for accelerating large-scale inverse problems. *arXiv preprint arXiv:2303.05754*, 2023.
- [26] Hyungjin Chung, Dohoon Ryu, Michael T McCann, Marc L Klasky, and Jong Chul Ye. Solving 3d inverse problems using pre-trained 2d diffusion models. In *Proceedings of the IEEE/CVF Conference on Computer Vision and Pattern Recognition*, pages 22542–22551, 2023.
- [27] Wenxiang Cong, Wenjun Xia, and Ge Wang. Image reconstruction from sparse low-dose ct data via score matching. *arXiv preprint arXiv:2306.08610*, 2023.
- [28] Florinel-Alin Croitoru, Vlad Hondru, Radu Tudor Ionescu, and Mubarak Shah. Diffusion models in vision: A survey. *IEEE transactions on pattern analysis and machine intelligence*, 45(9):1–20, 2023. ISSN 0162-8828.
- [29] Arthur P Dempster, Nan M Laird, and Donald B Rubin. Maximum likelihood from incomplete data via the EM algorithm. *Journal of the Royal Statistical Society: Series B (Methodological)*, 39(1):1–22, 1977.
- [30] David L Donoho. Compressed sensing. *IEEE Transactions on information theory*, 52(4):1289–1306, 2006.
- [31] Chenhe Du, Xiyue Lin, Qing Wu, Xuanyu Tian, Ying Su, Zhe Luo, Hongjiang Wei, S Kevin Zhou, Jingyi Yu, and Yuyao Zhang. Dper: Diffusion prior driven neural representation for limited angle and sparse view ct reconstruction. *arXiv preprint arXiv:2404.17890*, 2024.
- [32] Shiyi Du, Xiaosong Wang, Yongyi Lu, Yuyin Zhou, Shaoting Zhang, Alan Yuille, Kang Li, and Zongwei Zhou. Boosting dermatoscopic lesion segmentation via diffusion models with visual and textual prompts, 2023.
- [33] Paul Friedrich, Julia Wolleb, Florentin Bieder, Alicia Durrer, and Philippe C. Cattin. Wdm: 3d wavelet diffusion models for high-resolution medical image synthesis, 2024.
- [34] Ziqi Gao and S. Kevin Zhou. U²mrpd: Unsupervised undersampled mri reconstruction by prompting a large latent diffusion model, 2024.
- [35] Rongjun Ge, Yuting He, Cong Xia, Yang Chen, Daoqiang Zhang, and Ge Wang. Jccs-pfgm: A novel circle-supervision based poisson flow generative model for multiphase cect progressive low-dose reconstruction with joint condition, 2023.
- [36] Donald Geman and Chengda Yang. Nonlinear image recovery with half-quadratic regularization. *IEEE transactions on Image Processing*, 4(7):932–946, 1995.
- [37] Mengxiao Geng, Jiahao Zhu, Xiaolin Zhu, Qiqing Liu, Dong Liang, and Qiegen Liu. Dp-mdm: Detail-preserving mr reconstruction via multiple diffusion models, 2024. URL <https://arxiv.org/abs/2405.05763>.
- [38] Richard Gordon, Robert Bender, and Gabor T Herman. Algebraic reconstruction techniques (art) for three-dimensional electron microscopy and x-ray photography. *Journal of theoretical Biology*, 29(3):471–481, 1970.

- [39] Albert Gu and Tri Dao. Mamba: Linear-time sequence modeling with selective state spaces, 2024. URL <https://arxiv.org/abs/2312.00752>.
- [40] Yu Guan, Chuanming Yu, Zhuoxu Cui, Huilin Zhou, and Qiegen Liu. Correlated and multi-frequency diffusion modeling for highly under-sampled mri reconstruction. *IEEE Transactions on Medical Imaging*, 2024.
- [41] Alper Güngör, Salman UH Dar, Şaban Öztürk, Yilmaz Korkmaz, Hasan A Bedel, Gokberk Elmas, Muzaffer Ozbey, and Tolga Çukur. Adaptive diffusion priors for accelerated mri reconstruction. *Medical image analysis*, 88:102872, 2023.
- [42] Justin P Haldar and Jingwei Zhuo. P-loraks: low-rank modeling of local k-space neighborhoods with parallel imaging data. *Magnetic resonance in medicine*, 75(4):1499–1514, 2016.
- [43] Colin Hansen, Simas Glinskis, Ashwin Raju, Micha Kornreich, JinHyeong Park, Jayashri Pawar, Richard Herzog, Li Zhang, and Benjamin Odry. Inpainting pathology in lumbar spine mri with latent diffusion. *arXiv preprint arXiv:2406.02477*, 2024.
- [44] Jia He, Bonan Li, Ge Yang, and Ziwen Liu. Blaze3dm: Marry triplane representation with diffusion for 3d medical inverse problem solving, 2024. URL <https://arxiv.org/abs/2405.15241>.
- [45] Moein Heidari, Sina Ghorbani Kolahi, Sanaz Karimijafarbigloo, Bobby Azad, Afshin Bozorgpour, Soheila Hatami, Reza Azad, Ali Diba, Ulas Bagci, Dorit Merhof, and Ilker Hacihaliloglu. Computation-efficient era: A comprehensive survey of state space models in medical image analysis, 2024.
- [46] Dennis Hein, Staffan Holmin, Timothy Szczykutowicz, Jonathan S Maltz, Mats Danielsson, Ge Wang, and Mats Persson. Noise suppression in photon-counting ct using unsupervised poisson flow generative models, 2024.
- [47] Dennis Hein, Adam Wang, and Ge Wang. Poisson flow consistency models for low-dose ct image denoising, 2024.
- [48] Jonathan Ho, Ajay Jain, and Pieter Abbeel. Denoising diffusion probabilistic models. In H. Larochelle, M. Ranzato, R. Hadsell, M.F. Balcan, and H. Lin, editors, *Advances in Neural Information Processing Systems*, volume 33, pages 6840–6851. Curran Associates, Inc., 2020. URL https://proceedings.neurips.cc/paper_files/paper/2020/file/4c5bcfec8584af0d967f1ab10179ca4b-Paper.pdf.
- [49] Edward J Hu, Yelong Shen, Phillip Wallis, Zeyuan Allen-Zhu, Yuezhi Li, Shean Wang, Lu Wang, and Weizhu Chen. Lora: Low-rank adaptation of large language models. 2021.
- [50] Kun Huang, Xiao Ma, Yuhan Zhang, Na Su, Songtao Yuan, Yong Liu, Qiang Chen, and Huazhu Fu. Memory-efficient high-resolution oct volume synthesis with cascaded amortized latent diffusion models, 2024. URL <https://arxiv.org/abs/2405.16516>.
- [51] Phillip Isola, Jun-Yan Zhu, Tinghui Zhou, and Alexei A. Efros. Image-to-image translation with conditional adversarial networks. In *2017 IEEE Conference on Computer Vision and Pattern Recognition (CVPR)*, pages 5967–5976, 2017. doi:10.1109/CVPR.2017.632.
- [52] Hongxu Jiang, Muhammad Imran, Linhai Ma, Teng Zhang, Yuyin Zhou, Muxuan Liang, Kuang Gong, and Wei Shao. Fast denoising diffusion probabilistic models for medical image-to-image generation. *arXiv preprint arXiv:2405.14802*, 2024.
- [53] Zhihan Ju and Wanting Zhou. Vm-ddpm: Vision mamba diffusion for medical image synthesis, 2024.
- [54] Tero Karras, Miika Aittala, Timo Aila, and Samuli Laine. Elucidating the design space of diffusion-based generative models. In S. Koyejo, S. Mohamed, A. Agarwal, D. Belgrave, K. Cho, and A. Oh, editors, *Advances in Neural Information Processing Systems*, volume 35, pages 26565–26577. Curran Associates, Inc., 2022. URL https://proceedings.neurips.cc/paper_files/paper/2022/file/a98846e9d9cc01cfb87eb694d946ce6b-Paper-Conference.pdf.
- [55] Tero Karras, Miika Aittala, Timo Aila, and Samuli Laine. Elucidating the design space of diffusion-based generative models, 2022.
- [56] Amirhossein Kazerooni, Ehsan Khodapanah Aghdam, Moein Heidari, Reza Azad, Mohsen Fayyaz, Ilker Hacihaliloglu, and Dorit Merhof. Diffusion models in medical imaging: A comprehensive survey. *Medical image analysis*, 88:102846–102846, 2023. ISSN 1361-8415.
- [57] Dongjun Kim, Chieh-Hsin Lai, Wei-Hsiang Liao, Naoki Murata, Yuhta Takida, Toshimitsu Uesaka, Yutong He, Yuki Mitsufuji, and Stefano Ermon. Consistency trajectory models: Learning probability flow ODE trajectory of diffusion. In *The Twelfth International Conference on Learning Representations*, 2024. URL <https://openreview.net/forum?id=ymjI8feDTD>.

- [58] Jonghun Kim and Hyunjin Park. Adaptive latent diffusion model for 3d medical image to image translation: Multi-modal magnetic resonance imaging study. In *Proceedings of the IEEE/CVF Winter Conference on Applications of Computer Vision*, pages 7604–7613, 2024.
- [59] Nicholas Konz, Yuwen Chen, Haoyu Dong, and Maciej A. Mazurowski. Anatomically-controllable medical image generation with segmentation-guided diffusion models, 2024. URL <https://arxiv.org/abs/2402.05210>.
- [60] Alain Lalonde, Zhihao Chen, Thibaut Pommier, Thomas Decourselle, Abdul Qayyum, Michel Salomon, Dominique Ginjac, Youssef Skandarani, Arnaud Boucher, Khawla Brahim, Marleen de Bruijne, Robin Camarasa, Teresa M. Correia, Xue Feng, Kibrom B. Girum, Anja Hennemuth, Markus Huellebrand, Raabid Hussain, Matthias Ivantsits, Jun Ma, Craig Meyer, Rishabh Sharma, Jixi Shi, Nikolaos V. Tsekos, Marta Varela, Xiyue Wang, Sen Yang, Hannu Zhang, Yichi Zhang, Yuncheng Zhou, Xiahai Zhuang, Raphael Couturier, and Fabrice Meriaudeau. Deep learning methods for automatic evaluation of delayed enhancement-mri. the results of the emidec challenge, 2021.
- [61] Suhyeon Lee, Hyungjin Chung, Minyoung Park, Jonghyuk Park, Wi-Sun Ryu, and Jong Chul Ye. Improving 3d imaging with pre-trained perpendicular 2d diffusion models. In *Proceedings of the IEEE/CVF International Conference on Computer Vision*, pages 10710–10720, 2023.
- [62] Shudong Li, Xiao Jiang, Matthew Tivnan, Grace J Gang, Yuan Shen, and J Webster Stayman. Ct reconstruction using diffusion posterior sampling conditioned on a nonlinear measurement model. *ArXiv*, 2024.
- [63] Long Lian, Boyi Li, Adam Yala, and Trevor Darrell. Llm-grounded diffusion: Enhancing prompt understanding of text-to-image diffusion models with large language models, 2024.
- [64] Jörg Liesen and Zdenek Strakos. *Krylov subspace methods: principles and analysis*. Numerical Mathematics and Scie, 2013.
- [65] Yaron Lipman, Ricky TQ Chen, Heli Ben-Hamu, Maximilian Nickel, and Matt Le. Flow matching for generative modeling. *arXiv preprint arXiv:2210.02747*, 2022.
- [66] Anqi Liu, Grace J. Gang, and J. Webster Stayman. Fourier diffusion for sparse CT reconstruction. In Rebecca Fahrig, John M. Sabol, and Ke Li, editors, *Medical Imaging 2024: Physics of Medical Imaging*, volume 12925, page 1292516. International Society for Optics and Photonics, SPIE, 2024. doi:[10.1117/12.3008622](https://doi.org/10.1117/12.3008622). URL <https://doi.org/10.1117/12.3008622>.
- [67] Guan-Hong Liu, Arash Vahdat, De-An Huang, Evangelos A. Theodorou, Weili Nie, and Anima Anandkumar. I²sb: Image-to-image schrödinger bridge, 2023.
- [68] Xingchao Liu, Chengyue Gong, and Qiang Liu. Flow straight and fast: Learning to generate and transfer data with rectified flow. *arXiv preprint arXiv:2209.03003*, 2022.
- [69] Xuan Liu, Yaoqin Xie, Jun Cheng, Songhui Diao, Shan Tan, and Xiaokun Liang. Diffusion probabilistic priors for zero-shot low-dose ct image denoising, 2023.
- [70] Ziming Liu, Di Luo, Yilun Xu, Tommi Jaakkola, and Max Tegmark. Genphys: From physical processes to generative models. 2023.
- [71] Simian Luo, Yiqin Tan, Longbo Huang, Jian Li, and Hang Zhao. Latent consistency models: Synthesizing high-resolution images with few-step inference. 2023.
- [72] Morteza Mardani, Enhao Gong, Joseph Y. Cheng, Shreyas Vasanaawala, Greg Zaharchuk, Marcus Alley, Neil Thakur, Song Han, William Dally, John M. Pauly, and Lei Xing. Deep generative adversarial networks for compressed sensing automates mri, 2017. URL <https://arxiv.org/abs/1706.00051>.
- [73] Shanzhou Niu, Yang Gao, Zhaoying Bian, Jing Huang, Wufan Chen, Gaohang Yu, Zhengrong Liang, and Jianhua Ma. Sparse-view x-ray ct reconstruction via total generalized variation regularization. *Physics in Medicine & Biology*, 59(12):2997–3017, 2014.
- [74] Klaas P Pruessmann, Markus Weiger, Markus B Scheidegger, and Peter Boesiger. Sense: sensitivity encoding for fast mri. *Magnetic Resonance in Medicine: An Official Journal of the International Society for Magnetic Resonance in Medicine*, 42(5):952–962, 1999.
- [75] Albert W Reed, Hyojin Kim, Rushil Anirudh, K Aditya Mohan, Kyle Champley, Jingu Kang, and Suren Jayasuriya. Dynamic ct reconstruction from limited views with implicit neural representations and parametric motion fields. In *Proceedings of the IEEE/CVF International Conference on Computer Vision*, pages 2258–2268, 2021.
- [76] Robin Rombach, Andreas Blattmann, Dominik Lorenz, Patrick Esser, and Björn Ommer. High-resolution image synthesis with latent diffusion models. In *Proceedings of the IEEE/CVF Conference on Computer Vision and Pattern Recognition (CVPR)*, pages 10684–10695, June 2022.

- [77] Olaf Ronneberger, Philipp Fischer, and Thomas Brox. U-net: Convolutional networks for biomedical image segmentation, 2015. URL <https://arxiv.org/abs/1505.04597>.
- [78] Moiz Khan Sherwani and Shyam Gopalakrishnan. A systematic literature review: deep learning techniques for synthetic medical image generation and their applications in radiotherapy. *Frontiers in Radiology*, 4:1385742, 2024.
- [79] Peter J Shin, Peder EZ Larson, Michael A Ohliger, Michael Elad, John M Pauly, Daniel B Vigneron, and Michael Lustig. Calibrationless parallel imaging reconstruction based on structured low-rank matrix completion. *Magnetic resonance in medicine*, 72(4):959–970, 2014.
- [80] Nir Shlezinger, Yonina C Eldar, and Stephen P Boyd. Model-based deep learning: On the intersection of deep learning and optimization. *IEEE Access*, 10:115384–115398, 2022.
- [81] Ammar A. Siddiqui, Santosh Tirunagari, Tehseen Zia, and David Windridge. Vald-md: Visual attribution via latent diffusion for medical diagnostics, 2024.
- [82] Imraj RD Singh, Alexander Denker, Riccardo Barbano, Željko Kereta, Bangti Jin, Kris Thielemans, Peter Maass, and Simon Arridge. Score-based generative models for pet image reconstruction. *Machine Learning for Biomedical Imaging*, 2(Generative Models):547–585, January 2024. ISSN 2766-905X. doi:10.59275/j.melba.2024-5d51. URL <http://dx.doi.org/10.59275/j.melba.2024-5d51>.
- [83] Jascha Sohl-Dickstein, Eric Weiss, Niru Maheswaranathan, and Surya Ganguli. Deep unsupervised learning using nonequilibrium thermodynamics. In Francis Bach and David Blei, editors, *Proceedings of the 32nd International Conference on Machine Learning*, volume 37 of *Proceedings of Machine Learning Research*, pages 2256–2265, Lille, France, 07–09 Jul 2015. PMLR. URL <https://proceedings.mlr.press/v37/sohl-dickstein15.html>.
- [84] Jiaming Song, Chenlin Meng, and Stefano Ermon. Denoising diffusion implicit models. *arXiv preprint arXiv:2010.02502*, 2020.
- [85] Jiaming Song, Chenlin Meng, and Stefano Ermon. Denoising diffusion implicit models. In *International Conference on Learning Representations*, 2021. URL <https://openreview.net/forum?id=St1giarCHLP>.
- [86] Yang Song and Prafulla Dhariwal. Improved techniques for training consistency models. In *The Twelfth International Conference on Learning Representations*, 2024. URL <https://openreview.net/forum?id=WNzy9bRDvG>.
- [87] Yang Song and Stefano Ermon. Generative modeling by estimating gradients of the data distribution. In H. Wallach, H. Larochelle, A. Beygelzimer, F. d’Alché-Buc, E. Fox, and R. Garnett, editors, *Advances in Neural Information Processing Systems*, volume 32. Curran Associates, Inc., 2019. URL https://proceedings.neurips.cc/paper_files/paper/2019/file/3001ef257407d5a371a96dcd947c7d93-Paper.pdf.
- [88] Yang Song, Liyue Shen, Lei Xing, and Stefano Ermon. Solving inverse problems in medical imaging with score-based generative models. *arXiv preprint arXiv:2111.08005*, 2021.
- [89] Yang Song, Jascha Sohl-Dickstein, Diederik P Kingma, Abhishek Kumar, Stefano Ermon, and Ben Poole. Score-based generative modeling through stochastic differential equations. In *International Conference on Learning Representations*, 2021. URL <https://openreview.net/forum?id=PXTIG12RRHS>.
- [90] Yang Song, Prafulla Dhariwal, Mark Chen, and Ilya Sutskever. Consistency models. In *Proceedings of the 40th International Conference on Machine Learning*, ICML’23. JMLR.org, 2023.
- [91] Yang Song, Prafulla Dhariwal, Mark Chen, and Ilya Sutskever. Consistency models, 2023.
- [92] Niranjan Sridhar, Michael Elad, Carson McNeil, Ehud Rivlin, and Daniel Freedman. Diffusion models for generative histopathology. In *International Conference on Medical Image Computing and Computer-Assisted Intervention*, pages 154–163. Springer, 2023.
- [93] Shobhita Sundaram and Neha Hulkund. Gan-based data augmentation for chest x-ray classification, 2021.
- [94] Jie Tang, Brian E Nett, and Guang-Hong Chen. Performance comparison between total variation (tv)-based compressed sensing and statistical iterative reconstruction algorithms. *Physics in Medicine & Biology*, 54(19):5781, 2009.
- [95] Chameleon Team. Chameleon: Mixed-modal early-fusion foundation models. *arXiv preprint arXiv:2405.09818*, 2024.
- [96] Matthew Tivnan, Jacopo Teneggi, Tzu-Cheng Lee, Ruoqiao Zhang, Kirsten Boedeker, Liang Cai, Grace J Gang, Jeremias Sulam, and J. Webster Stayman. Fourier diffusion models: A method to control mtf and nps in score-based stochastic image generation. 2023.

- [97] Payal Varshney, Adriano Lucieri, Christoph Balada, Andreas Dengel, and Sheraz Ahmed. Generating counterfactual trajectories with latent diffusion models for concept discovery. *arXiv preprint arXiv:2404.10356*, 2024.
- [98] Ashish Vaswani, Noam Shazeer, Niki Parmar, Jakob Uszkoreit, Llion Jones, Aidan N Gomez, Łukasz Kaiser, and Illia Polosukhin. Attention is all you need. In I. Guyon, U. Von Luxburg, S. Bengio, H. Wallach, R. Fergus, S. Vishwanathan, and R. Garnett, editors, *Advances in Neural Information Processing Systems*, volume 30. Curran Associates, Inc., 2017. URL https://proceedings.neurips.cc/paper_files/paper/2017/file/3f5ee243547dee91fbd053c1c4a845aa-Paper.pdf.
- [99] Corentin Vazia, Alexandre Bousse, Béatrice Vedel, Franck Vermet, Zhihan Wang, Thore Dassow, Jean-Pierre Tasu, Dimitris Visvikis, and Jacques Froment. Diffusion posterior sampling for synergistic reconstruction in spectral computed tomography, 2024.
- [100] Pascal Vincent. A connection between score matching and denoising autoencoders. *Neural computation*, 23(7): 1661–1674, 2011. ISSN 0899-7667.
- [101] Yuang Wang, Siyeop Yoon, Pengfei Jin, Matthew Tivnan, Zhenhong Chen, Rui Hu, Li Zhang, Zhiqiang Chen, Quanzheng Li, and Dufan Wu. Implicit image-to-image schrodinger bridge for ct super-resolution and denoising, 2024.
- [102] Tobias Weber, Michael Ingrisch, Bernd Bischl, and David Rügamer. Cascaded latent diffusion models for high-resolution chest x-ray synthesis, 2023.
- [103] Haoyu Wei, Florian Schiffrers, Tobias Würfl, Daming Shen, Daniel Kim, Aggelos K. Katsaggelos, and Oliver Cossairt. 2-step sparse-view ct reconstruction with a domain-specific perceptual network, 2020. URL <https://arxiv.org/abs/2012.04743>.
- [104] Julia Wolleb, Robin Sandkühler, Florentin Bieder, Philippe Valmaggia, and Philippe C. Cattin. Diffusion models for implicit image segmentation ensembles, 2021.
- [105] Junde Wu, Rao Fu, Huihui Fang, Yu Zhang, Yehui Yang, Haoyi Xiong, Huiying Liu, and Yanwu Xu. Medsegdiff: Medical image segmentation with diffusion probabilistic model, 2023.
- [106] Junde Wu, Wei Ji, Huazhu Fu, Min Xu, Yueming Jin, and Yanwu Xu. Medsegdiff-v2: Diffusion based medical image segmentation with transformer, 2023.
- [107] Qing Wu, Ruimin Feng, Hongjiang Wei, Jingyi Yu, and Yuyao Zhang. Self-supervised coordinate projection network for sparse-view computed tomography. *IEEE Transactions on Computational Imaging*, 9:517–529, 2023.
- [108] Wenjun Xia, Wenxiang Cong, and Ge Wang. Patch-based denoising diffusion probabilistic model for sparse-view ct reconstruction. *arXiv preprint arXiv:2211.10388*, 2022.
- [109] Wenjun Xia, Chuang Niu, Wenxiang Cong, and Ge Wang. Sub-volume-based denoising diffusion probabilistic model for cone-beam ct reconstruction from incomplete data. *Computing Research Repository (CoRR)*, 2023.
- [110] Huidong Xie, Weijie Gan, Bo Zhou, Ming-Kai Chen, Michal Kulon, Annemarie Boustani, Benjamin A Spencer, Reimund Bayerlein, Xiongchao Chen, Qiong Liu, et al. Dose-aware diffusion model for 3d low-dose pet: Multi-institutional validation with reader study and real low-dose data. *arXiv preprint arXiv:2405.12996*, 2024.
- [111] Zhuang Xiong, Wei Jiang, Yang Gao, Feng Liu, and Hongfu Sun. Qsmdiff: Unsupervised 3d diffusion models for quantitative susceptibility mapping, 2024.
- [112] Rui Xu, Yunke Wang, and Bo Du. Maediff: Masked autoencoder-enhanced diffusion models for unsupervised anomaly detection in brain images, 2024.
- [113] Yilun Xu, Ziming Liu, Max Tegmark, and Tommi Jaakkola. Poisson flow generative models. In S. Koyejo, S. Mohamed, A. Agarwal, D. Belgrave, K. Cho, and A. Oh, editors, *Advances in Neural Information Processing Systems*, volume 35, pages 16782–16795. Curran Associates, Inc., 2022. URL https://proceedings.neurips.cc/paper_files/paper/2022/file/6ad68a54eaa8f9bf6ac698b02ec05048-Paper-Conference.pdf.
- [114] Yilun Xu, Ziming Liu, Yonglong Tian, Shangyuan Tong, Max Tegmark, and Tommi Jaakkola. PFGM++: Unlocking the potential of physics-inspired generative models. In Andreas Krause, Emma Brunskill, Kyunghyun Cho, Barbara Engelhardt, Sivan Sabato, and Jonathan Scarlett, editors, *Proceedings of the 40th International Conference on Machine Learning*, volume 202 of *Proceedings of Machine Learning Research*, pages 38566–38591. PMLR, 23–29 Jul 2023. URL <https://proceedings.mlr.press/v202/xu23m.html>.
- [115] Guoqiang Yu, Liang Li, Jianwei Gu, and Li Zhang. Total variation based iterative image reconstruction. In *International Workshop on Computer Vision for Biomedical Image Applications*, pages 526–534. Springer, 2005.

- [116] Lijun Yu, José Lezama, Nitesh B. Gundavarapu, Luca Versari, Kihyuk Sohn, David Minnen, Yong Cheng, Vighnesh Birodkar, Agrim Gupta, Xiuye Gu, Alexander G. Hauptmann, Boqing Gong, Ming-Hsuan Yang, Irfan Essa, David A. Ross, and Lu Jiang. Language model beats diffusion – tokenizer is key to visual generation, 2024.
- [117] Pengxin Yu, Haoyue Zhang, Han Kang, Wen Tang, Corey W Arnold, and Rongguo Zhang. Rplhr-ct dataset and transformer baseline for volumetric super-resolution from ct scans. In *International Conference on Medical Image Computing and Computer-Assisted Intervention*, pages 344–353. Springer, 2022.
- [118] Guangming Zang, Ramzi Idoughi, Rui Li, Peter Wonka, and Wolfgang Heidrich. Intratomo: self-supervised learning-based tomography via sinogram synthesis and prediction. In *Proceedings of the IEEE/CVF International Conference on Computer Vision*, pages 1960–1970, 2021.
- [119] Chenlu Zhan, Yu Lin, Gaoang Wang, Hongwei Wang, and Jian Wu. Medm2g: Unifying medical multi-modal generation via cross-guided diffusion with visual invariant. In *Proceedings of the IEEE/CVF Conference on Computer Vision and Pattern Recognition*, pages 11502–11512, 2024.
- [120] Hanming Zhang, Liang Li, Kai Qiao, Linyuan Wang, Bin Yan, Lei Li, and Guoen Hu. Image prediction for limited-angle tomography via deep learning with convolutional neural network. *arXiv preprint arXiv:1607.08707*, 2016.
- [121] Hantao Zhang, Jiancheng Yang, Shouhong Wan, and Pascal Fua. Lefusion: Synthesizing myocardial pathology on cardiac mri via lesion-focus diffusion models, 2024.
- [122] Kejia Zhang, Lan Zhang, Haiwei Pan, and Baolong Yu. Cts: A consistency-based medical image segmentation model, 2024.
- [123] Ling Zhang, Xiaosong Wang, Dong Yang, Thomas Sanford, Stephanie Harmon, Baris Turkbey, Bradford J. Wood, Holger Roth, Andriy Myronenko, Daguang Xu, and Ziyue Xu. Generalizing deep learning for medical image segmentation to unseen domains via deep stacked transformation. *IEEE Transactions on Medical Imaging*, 39(7):2531–2540, 2020. doi:[10.1109/TMI.2020.2973595](https://doi.org/10.1109/TMI.2020.2973595).
- [124] Tianyi Zhang, Zheng Wang, Jing Huang, Mohiuddin Muhammad Tasnim, and Wei Shi. A survey of diffusion based image generation models: Issues and their solutions. 2023.
- [125] Yuxin Zhang, Clément Huneau, Jérôme Idier, and Diana Mateus. Ultrasound image reconstruction with denoising diffusion restoration models. In *International Conference on Medical Image Computing and Computer-Assisted Intervention*, pages 193–203. Springer, 2023.
- [126] Yuxin Zhang, Clément Huneau, Jérôme Idier, and Diana Mateus. Ultrasound imaging based on the variance of a diffusion restoration model. *arXiv preprint arXiv:2403.15316*, 2024.
- [127] Jian-Qing Zheng, Yuanhan Mo, Yang Sun, Jiahua Li, Fuping Wu, Ziyang Wang, Tonia Vincent, and Bartłomiej W Papież. Deformation-recovery diffusion model (drdm): Instance deformation for image manipulation and synthesis. *arXiv preprint arXiv:2407.07295*, 2024.
- [128] Tao Zhou, Huazhu Fu, Geng Chen, Jianbing Shen, and Ling Shao. Hi-net: hybrid-fusion network for multi-modal mr image synthesis. *IEEE transactions on medical imaging*, 39(9):2772–2781, 2020.
- [129] Lingting Zhu, Zeyue Xue, Zhenchao Jin, Xian Liu, Jingzhen He, Ziwei Liu, and Lequan Yu. Make-a-volume: Leveraging latent diffusion models for cross-modality 3d brain mri synthesis. In *International Conference on Medical Image Computing and Computer-Assisted Intervention*, pages 592–601. Springer, 2023.
- [130] Lingting Zhu, Noel Codella, Dongdong Chen, Zhenchao Jin, Lu Yuan, and Lequan Yu. Generative enhancement for 3d medical images. *arXiv preprint arXiv:2403.12852*, 2024.